Safety in Mines Research Advisory Committee

Final Project Report

The meaningful use of peak particle velocity at excavation surface for the optimisation of the rockburst support criteria for tunnels and stopes

A. Cichowicz

Research agency	:	ISS International Limited
Project number	:	GAP 709b
Project duration	:	2000/04 - 2001/03
Report date	:	March 2001

Executive summary

A set of data, collected from Mponeng and East Driefontein Mines, provides a new insight into the response of support units under seismic load. The most important accomplishment of monitoring is the measurement of peak ground acceleration caused by strong ground motion in the hangingwall, footwall and support units. The strongest monitored peak ground accelerations are in the range of 70 - 118m/s^2 which, after integration, relate to peak ground velocity in the range of 0.34 - 0.46 m/s. These parameters of strong ground motion are caused by seismic events of magnitude 1.2 - 2.4 observed from distances of 80 - 140m. The strongest ground motion was monitored by horizontal accelerometers and not, as could be expected, by vertical ones.

A semi-empirical model of peak ground velocity (PGV) is proposed to predict the ground motion of future seismic events. The attenuation curve for the PGV quantifies the effect of source, distance between source and site, and site amplification at the stope. The ground motion of moderate seismic events with magnitude 0.7 and 1.2 is amplified in the stope, however ground motion generated by a large seismic event with magnitude 2.4 is not amplified in the stope. This statement is based on three independent estimations.

Data shows that support response to strong ground motion has radically different characteristics compared to support response to weak ground motion. The weak ground motion reveals a total lack of coherence between ground motions in the hangingwall and footwall. Weak ground motion does not cause permanent deformation in the stope as it carries a mostly high frequency signal. Weak ground motion causes support response only in its elastic range and provides no information about what happens in a range of plastic deformations.

The near-field strong ground motion data provides a base for proposing a new model of support response due to seismic loading. The cyclic response of the support (brick composite pack) to cyclic seismic loading was unexpected. Observed vibrations of the support indicate that some portion of energy impacted into the support will be returned to the surrounding rock. This means that the entire input energy is not converted into permanent deformation. Therefore, the area under a load-deformation curve, calculated from zero to a value of maximal vertical displacement, does not measure the energy absorbed by support, because most of the input energy is returned to the surrounding rock. The Handbook on Rock Engineering Practice for Tabular Hard Rock Mines suggests that seismic input energy has to be absorbed by support. The capacity of support to absorb energy is equal to the area under a load-displacement curve. This relationship correctly estimates a maximal possible displacement of support during a seismic event, however, it is not suitable to estimate the energy absorbed by support under a seismic load, as it is claimed. The source of confusion is when ground motion caused by a seismic event is understood as a monotonic dynamic load, so that it can be modelled, for example, using an experiment with a press. Seismic ground motion has a cyclic behaviour.

Acknowledgements

Site selection and data collection would have been impossible without help from Mr A. Ward and Mr D. Pretorius from Mponeng Mine, Mr R Ferreira and Mr D. Rossouw from East Driefontein Mine. Discussions with them were also of great value. Thanks also to Mr D. Adams for critically reading the manuscript.

Table of contents

List of figures

List of tables

1. Introduction

The waveforms of strong ground motion are required to design the optimal stope support in seismically active areas.

The primary output of the project is analysis of relationships between ground motion recorded at the walls of the stope, seismic source parameters and the geotechnical parameters of the stope. These relationships will form the basis of a guideline for optimal rockburst support criteria.

The structure of the report follows the objectives selected in the project proposal and during the course of the project. Due to the unexpected behaviour of stope support under seismic load, an additional task was formulated. The final list of objectives reads as follows:

- Maintenance of seismic instrumentation and building a data base of ground motion recorded at the surfaces of the stope. (Chapter 2)

- Ground motion model of peak ground velocity (PGV) and/or peak ground acceleration (PGA) (Chapter 3 and 4)
    - Testing different empirical models of PGV and/or PGA. The models have to capture the relationship between ground motion parameters observed at the wall of an excavation, seismic source parameters and the distance between source and station. (Chapter 3)
    - For support design it is important to understand the frequency band in which the PGV and PGA will occur. For this purpose, the standard spectrum shape of the excavation is calculated. (Chapter 4)

- Support response to seismic load. Research focuses on the study of waveforms recorded in stope support and ground motion in the hangingwall and footwall. (Chapters 5 and 6)

The secondary output is the development of technology and procedures for the measurement of strong ground motion in general, as well as, stope and support response to dynamic load caused by peak ground acceleration and peak ground velocity.

Measurements with the differential accelerometer were done as planed (see previous progress reports). During data interpretation it became apparent, that the results were unreliable. The required differential acceleration information was, instead, determined through the set of sensors with three vertical components. (Chapter 5).

1.1. Literature search

For several typical structures some codes and standards have been developed to guide civil engineers to incorporate ground motion parameters into their particular designs (for example on 5 March 1999, The South African Bureau of Standards accepted ISO4866 Mechanical vibration and shock guidelines for the measurement of vibrations and the evaluation of their effects on buildings).

To meet safety standards for stope excavation we have to work persistently in the following fields:

- Develop techniques for the of extrapolation/prediction of ground motion at stope hangingwall and footwall, especially to predict the effects of larger events.
- Study the response of a stope and support exposed to dynamic conditions.

The ground motion caused by a seismic event is controlled by properties of the seismic source, propagation path and site effect at the recording station. The relationship between the ground motion parameters (peak ground velocity and peak ground acceleration, associated frequencies and duration of strong ground motion), seismic source parameters and ray path parameters are being extensively studied in crustal seismology.

In the mines, we need to quantify the effect of the geotechnical parameters of an excavation on ground motion. The effect of the excavation on ground motion parameters has to be quantified by building a model of the PGV and/or PGA. It will not be possible to have one model, that could describe all complex

phenomena around a site, but it will be possible to identify the most dominant parameters surrounding a stope. In previous studies of the site effect of excavations, effort was directed towards understanding the detail of ground motion. The task of separating the source effect, ray path, resonance and the mixture of body and surface waves is a difficult one. This project should focus on the generalisation of the source and propagation processes. Generalisations are useful for the estimation of future ground motion since details are not repeatable from one event to the next.

To predict PGV or PGA a specification of a basic spectral shape representing the radiation from the source is required. A number of frequency functions are needed to specify the observed spectra. The spectrum is modelled as a product of function modelling the source spectrum, function modelling the attenuation, and function modelling site effect at the wall of the stope. The rms acceleration, a_{rms} over the time interval carrying the S wave is defined as an integral of the squared acceleration. The Parseval theorem allows expression of a_{rms} as an integral of the squared acceleration spectrum. Using the Brune model of source spectrum a_{rms} is controlled by corner frequency, stress drop and radiation pattern distance. *McGuire and Hanks* (*1980*) first introduced the relation. An analogous expression was developed for v_{rms} velocity by *Atkinson* (*1984*). The random vibration theory relates the a_{rms} to the PGA and v_{rms} to the PGV. The essence of this method is to use whatever seismological information is available to specify the spectrum of the radiated energy, and then use the assumption that this energy is distributed in a random fashion over a duration related to the source duration. The PGA and PGV can be calculated knowing seismic moment (or magnitude), corner frequency, distance between source and station. This approach to estimate PGV or PGA is the most popular and powerful technique used in earthquake seismology. There is only one limitation, that is, several oscillations should be observed on a seismogram in order to justify the use of random vibration theory. The seismograms recorded in a stope with the strongest ground motions have only two or, a maximum of, three full cycles of oscillation. Therefore this excellent theory developed for modelling PGV and PGA in the far field is not applicable when modelling strong ground motion in a stope.

Only seismic data from the hangingwall, footwall and stope support provide relevant information about the behaviour of support under dynamic conditions. A blast could not be used to simulate ground motion parameters of a seismic event as it has a different frequency content, radiation pattern and essentially a different ray path. The blast is useful for analysing of rock behaviour under stress, but has a limited application in the study of site effect as a result of seismicity. In laboratory conditions support is subjected to monotonic loading while seismic loading has a cyclic behaviour.

What do we know so far about ground motion amplification at the wall of excavation?

Ortlepp (*1993*) presented a broad review of the literature. Due to lack of seismic observations in stopes damaged by seismic events, he refers mostly to indirect hypotheses about ground motion parameters (e.g. Wagner 1984).

The most significant contribution to the understanding of the scaling law governing the PGV and PGA recorded in solid rock, is given by *McGarr* (*1981*).

Linkov and Durrheim (*1998*) proved a theoretical explanation for peak ground velocity amplification. A mechanism of energy release, which emphasises the role of softening at interacting surfaces is proposed. The amplification occurs due to physical nonlinearity at interacting softening surfaces. This mechanism effects amplification mostly in the frequency range above 5000Hz.

Ground motion measurements made on the skin of the excavation indicate four- to ten-fold magnification of the peak velocity when compared to measurements within the solid rock at similar distances from the source (*Butler and van Aswegen, 1993*; GAP 201, *Cichowicz et al. 1999*, and *2000*).

The response of the structure surrounding an excavation is very complex in the high frequency range. Several resonance peaks from 200Hz to 2000 Hz can be observed. (GAP530, *Cichowicz et al. 1999*).

In analysed cases the amplification of a body wave signal starts from 40 Hz and amplification of a surface wave starts from 20-30 Hz. In some cases, at 60 Hz the influence of the stope on body waves is not seen at all (GAP530; *Cichowicz et al. 2000*). This discrepancy is caused by the horizontal dimension of the stope, the extent of inhomogenities in the vicinity of the stope and the location of the seismic source with respect to the station.

The local structure can generate channel ways with low frequency, not seen in body waves. These channel waves are responsible for the maximal peak ground velocity.

The fractured rock surrounding the stope causes scattering of seismic waves (*Cichowicz and Green 1989; Cichowicz et al. 1988*).

2. Data base description and logistic issues

Due to the lack of freely available, cost effective strong ground motion monitoring systems in the past, there is a lack of strong ground motion recording. Also, there is a complete lack of strong ground motion recordings at low frequency. It was proposed, that some newly developed instrumentation be applied to record strong ground motion data.

The recording instruments were placed in a stope of Driefontein Mine and Mponeng Mine. A recording seismometer (RS) with three vertical accelerometers, three component accelerometers and differential accelerometers were installed. The RSs are small and portable and a set of sensors can be installed in one day at any selected site. During the experiment the instruments followed the advancing of face. To establish the nature of stope hangingwall (fracture patterns, delamination thickness), a radar survey was conducted.

Collecting relevant data is a difficult process. The damaging strong ground motions are usually caused by events with magnitude larger than 1 and recorded at a distance of several dozen meters from a seismic source. To be at the right time and place required the close co-operation of an experienced rock mechanic practitioner.

The experimental part of the project was conducted at East Driefontein Mine, stope 30/31 VCR. Stope 30/31 is supported with backfill. The distance between the face and the first row of packs is 3.8 m. A distance between the hanging wall and footwall is, on average, 1.1 m. The seismic instruments have been installed some 10 m from the stope face next to wooden packs, between the third and four row of packs. After the site was selected the recording of data stared on the 4th of August 2000. On the 21st of September the whole set-up moved closer to the stope face. Packs where data acquisition units were mounted were significantly damaged. The new site was also located some10 m behind the face, next to a gully.

Initially, the differential accelerometer was cemented to the hangingwall and footwall, 0.4m from a wooden pack. Units with three vertical accelerometers (VA) have two components installed next to differential accelerometers and the third vertical component is cemented to the hanging wall, 2 m apart. Next to it there is a unit with a three-component accelerometer. The instruments were installed in this compact configuration to enable the control of measurements in the testing phase, and to gain some insight into the precision of observations.

After several weeks of successful monitoring it was realised that collection of data could occur concurrently from two sites. One of three units installed in East Driefontein Mine containing three vertical accelerometers was moved to Mponeng Mine. On October 18, a new site was established in Mponeng Mine, section 123, panel West 4 (W4), cross cut 48, level 99 (see Figure 2.1). The W4 is located next to a dyke. The W4 panel stopped in the beginning of October, as exploitation from the opposite direction was approaching towards the W4, and it stopped at a distance of some 30m from the face of it. Seismic sensors were installed some 4-5 m from face, near the brick composite pack and in the pack. On December 14, the experiment moved to panel W2, to be closer to active exploitation.

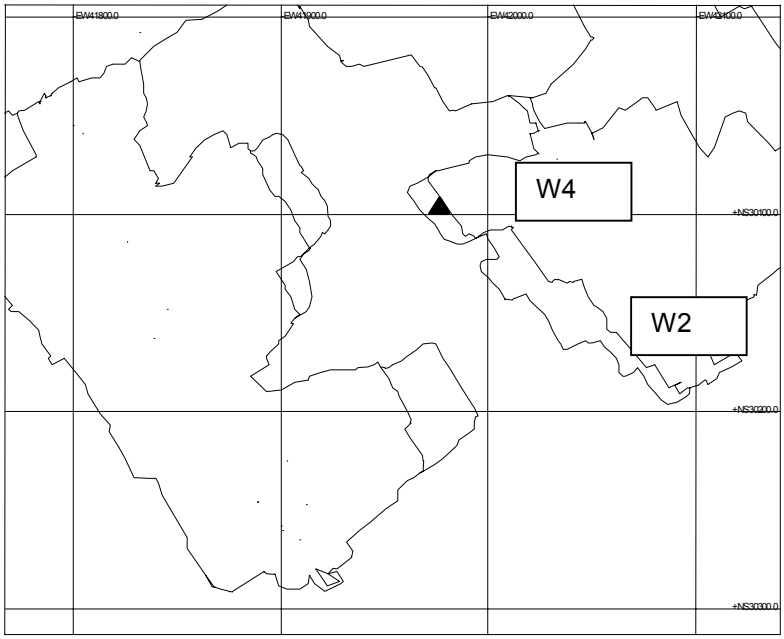

Figure 2.1. Plan view of section 123, Mponeng Mine, triangle displays location of experiment,W4. Face outlines as of November 2000 are shown.

The experiment at Mponeng Mine was conducted using three configurations of sensors. In the first configuration two sensors were attached to a footwall and one to a hangingwall. Most of the time accelerometers were placed as follows: one in the middle of the support, one at the hangingwall and one at the footwall (second configuration). For a limited time interval an additional unit of accelerometers was placed in the support (third configuration). One accelerometer was always installed in the middle of a pack, some 1.6 m above the footwall. The additional accelerometers were placed 0.2 m below the hangingwall and 0.4 m above footwall. The pack height was 2.3 m.

At one stage of the experiment at Driefontein Mine, a data acquisition unit with one vertical and two horizontal components recorded a very strong ground motion. This indicated, that the motion of stope hangingwall could have a horizontal component as strong as the vertical one. Additional motivation for using sensors with horizontal components was to help to locate the seismic events. However, with the cooperation of the mine seismologist, it was possible to associate the record of strong ground motion with a seismic event located by the mine's seismic network. Therefore, at the beginning of October 2000 it was decided to use a spare sensors and replaced the unit with one consisting of three vertical components. The sensors were installed at the hangingwall, footwall and on the support unit. This configuration of sensors addresses the problem of understanding the damaging phenomena in the most efficient way. After this re-arrangement it was possible to record at two different sites at the same time, as the other unit with three vertical components was still in operation.

During the course of the experiment some extra effort and time were dedicated to evaluating undesired site effects at the point of sensor installation. A site effect can originate from defective cementing of seismic sensors to the free surface of the hangingwall or footwall and from vibration of loose rock in extensively fractured surroundings. Experience shows that the cementing does not cause a problem. The best spot for the installation of the accelerometers was selected with the help of rock engineering staff on the mine. Two sensors were installed two meters apart in the footwall to evaluate the influence of local site effects. This experiment shows that the major features of accelerograms are preserved. In Mponeng Mine, observations were conducted in one place for a period of three months. To ensure that loose rocks did not systematically influence data, sensors were moved 3 m around the pack in two week cycles.

Monitoring with continuos differential units was less successful. Due to several independent logistic problems sensors were damaged twice, and as a result, several weeks of observation were lost. From the beginning of December 2000 a continuous differential unit was in operation underground.

Two types of sensors were tested, the first one with a dynamic range of 10 g and the second with a dynamic range of 50 g. On the basis of a pilot experiment it was decided to use a 50 g accelerometer, yet during laboratory tests with the 50 g accelerometer it was found to be a very stiff system. The 50 g accelerometer could not be excited with a geophysical hammer or small explosive. During the second stage, experiments were conducted underground, 10 m from the stope face. The 10 g accelerometer has amplitude characteristics shifted towards higher frequency. This is an undesired effect in an experiment that has to focus on the recording of large, damaging events. Therefore, after three weeks of experimentation, it was decided to base the experiment on 50 g accelerometers. This is an important finding as, by comparison, engineering seismologists that work with surface ground motion usually base their experiments on 2 g accelerometers.

Each seismic event is described using the following parameters: date, time, PGA, a distance between source and station, co-ordinates of the event, magnitude, log of seismic moment [Nm], log of seismic energy [J]. Table A1, A2 and A3 in Appendix 1 display the PGA measured at footwall (F), hangingwall (H) and support (S) for three configurations of sensors. The data base also has several records of a series of blasts, however they are not included in Table A1, A2, A3.

3. Ground motion model of peak ground velocity

The values of PGV and PGA play a central role in engineering applications. The recently collected database has several significant accelerograms recorded in the near source region. The goal is to test different empirical models of PGV. The attenuation models have to capture the relationship between ground motion parameters observed at the wall of an excavation, seismic source parameters and the distance between source and station.

In previous studies of the site effect of excavations an effort was directed towards understanding the detail of ground motion (*Cichowicz et al., 1999 and Cichowicz et al., 2000*). The task of separation of the source effect, ray path, resonance and the mixture of body and surface waves is a difficult one. The technology exists to calculate a synthetic seismogram using near field, intermediate field and far field components. Synthetic seismograms could be calculated at the skin of the excavation for all possible mechanisms and locations of seismic sources. This approach is highly impractical for the estimation of ground motion of future seismic events since details are not repeatable from one event to the next. Instead, the work is focused on the generalisation of the source, propagation processes and stope environment. The stope is quantified with a magnification factor which is a simple stope specific parameter.

The crucial step in the development of the attenuation curve is the selection of a mathematical model. *Campbell* (*1985*) has described the general forms of regression models of attenuation. The general form of the attenuation relations expresses peak ground parameters as a product of the following components: a function of seismic event magnitude, a function of distance, a joint function of magnitude and distance, a function representing parameters of the seismic event, path and random variable representing uncertainty.

Four ground motion models of PGV were developed and tested in this study. For detailed analysis, four seismic events are selected with high quality seismograms recorded in stope and by the mining network at the same time. The range of distances between source and station varies from 70m to 3000m. These distances relate to far field and near field zone of radiation pattern and therefore the empirical attenuation curve has to capture two different types of physical relationships.

The first PGV is estimated using empirical relationship which coefficients are based on regression analysis given by

$$V(R)=\frac{V_o}{R}\exp(-\alpha R) \qquad \textbf{(1)}$$

where R is the distance between seismic source and seismic station, V(R) is the PGV as a function of distance, Vo is the constant, α is the attenuation coefficient.

Figure 3.1 shows PGV data and attenuation curve for four events. The circle symbol is used to mark a PGV recorded by geophones at the mine network, asterisks indicate a PGV recorded in the hangingwall and footwall of a stope. The PGVs in the stope hangingwall and footwall are obtained from accelerograms using the integration procedure described in Appendix 2. The solid line shows the attenuation curve given by equation 1.The PGVs recorded in the stope are not included in building the model of the attenuation curve. Parameters Vo and α are obtained using least square estimation, the dashed line produces an error bounds, which give confidence intervals of 90%. It should be noticed, that scattering of data is large so the 90% confidence intervals vary almost 10 times up and 10 down from the model. The results for four seismic events are tabulated in Table 3.1. From visual inspection of Figure 3.1 it is clear, that model 1 could not be use to predict strong ground motion in a stope. There is a significant difference between the values of PGV predicted by the attenuation model and the values of PGV measured in the stope. This difference does not reflect a site amplification in the stope but rather indicates a strong difference in the attenuation model governing the far field and the near source region.

Table 3.1 Source parameters and attenuation parameters calculated for four seismic events where M_o is the seismic moment, f_o is the corner frequency of the S-wave, $\Delta\sigma$ is the static stress drop*.

	Mag	M_o [Nm]	f_o [Hz]	$\Delta\sigma$ [Pa]	Model 1 α	Model 2 n	Model 3 Q=200 n	Model 4 Q =200 n
1	1.2	$1.7\ 10^{11}$	20	$2.7\ 10^{5}$	0.00045	1.62	1.52	1.5
2	0.7	$3.9\ 10^{10}$	28	$1.9\ 10^{5}$	0.00010	1.67	1.56	1.5
3	2.4	$3.4\ 10^{12}$	14	$1.8\ 10^{5}$	0.00009	0.98	0.81	1.5
4	1.2	$1.7\ 10^{11}$	22	$4.6\ 10^{5}$	0.00011	1.67	1.54	1.5

* - M is the seismic moment, that is a product of rigidity modulus of the faulted medium, the average slip across a seismic source and area of seismic source,
- f_o is the corner frequency, which is a parameter of spectra reciprocal of seismic source size,
- Q is the quality factor, which is a reciprocal measure of attenuation (low Q value, that is strong attenuation)

Visual inspection of Figure 3.2 suggests that the straight line in a log-log graph could fit to data collected in the far field and in the stope quite well. The following model was tested

$$V(R) = \frac{V_o}{R^n} \qquad \textbf{(2)}$$

The least square fit was applied to four sets of seismograms. Figure 3.2 shows that this simple model developed using data only from the far field predicted ground motion in the near field better than Figure 3.1. The remarkable feature is that three events have the same value decay constant, n=1.6. The different decay constant has event 3 n = 1, which is the strongest one and has the lowest corner frequency of 14Hz. These facts indicate clearly, that attenuation of seismic waves is controlled by the dominant frequency of the seismic signal. The low frequencies signal of event 3 is attenuated more slowly than the high frequencies signal of the remaining seismic events.

One problem existing in the evaluation of attenuation curves is an ambiguity in the physical meanings of the formulations. In model 2, the decay constant "n" counts for geometrical spreading, attenuation due to inelasticity and near field components of the radiation pattern.

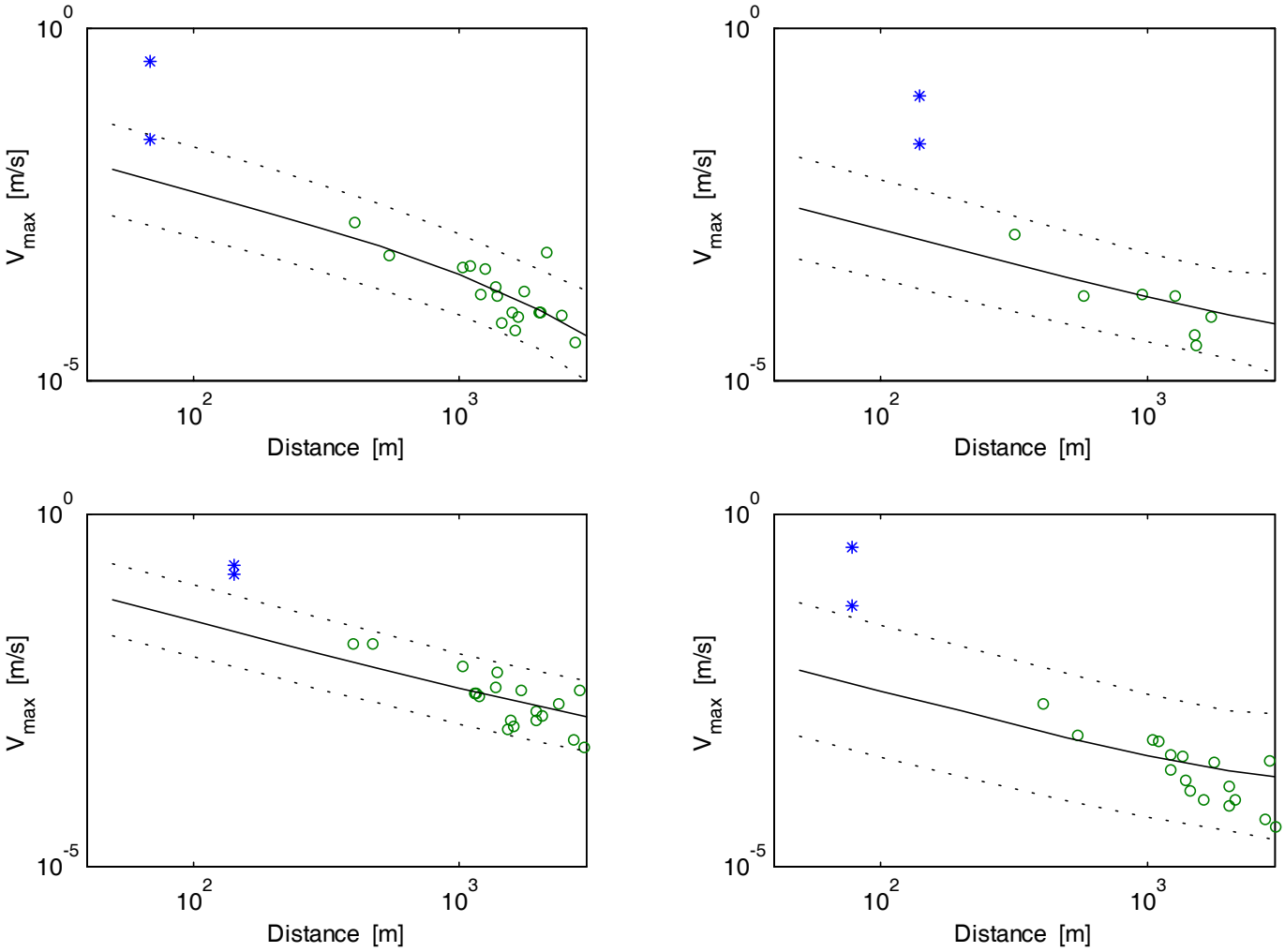

where the symbol of a circle is used to mark PGV recorded by geophones, asterisks indicate the PGV recorded in the hangingwall and footwall of the stope. The solid line shows the attenuation curve given by equation 1, using only data recorded by geophones, the dashed line produces an error bounds, which give confidence intervals of 90%. There is the following relation between numbers in the first column of Table 3.1 and graphs on Figure 3.1: event 1 - top left, event 2 - top right, event 3 - bottom left, event 4 - bottom right.

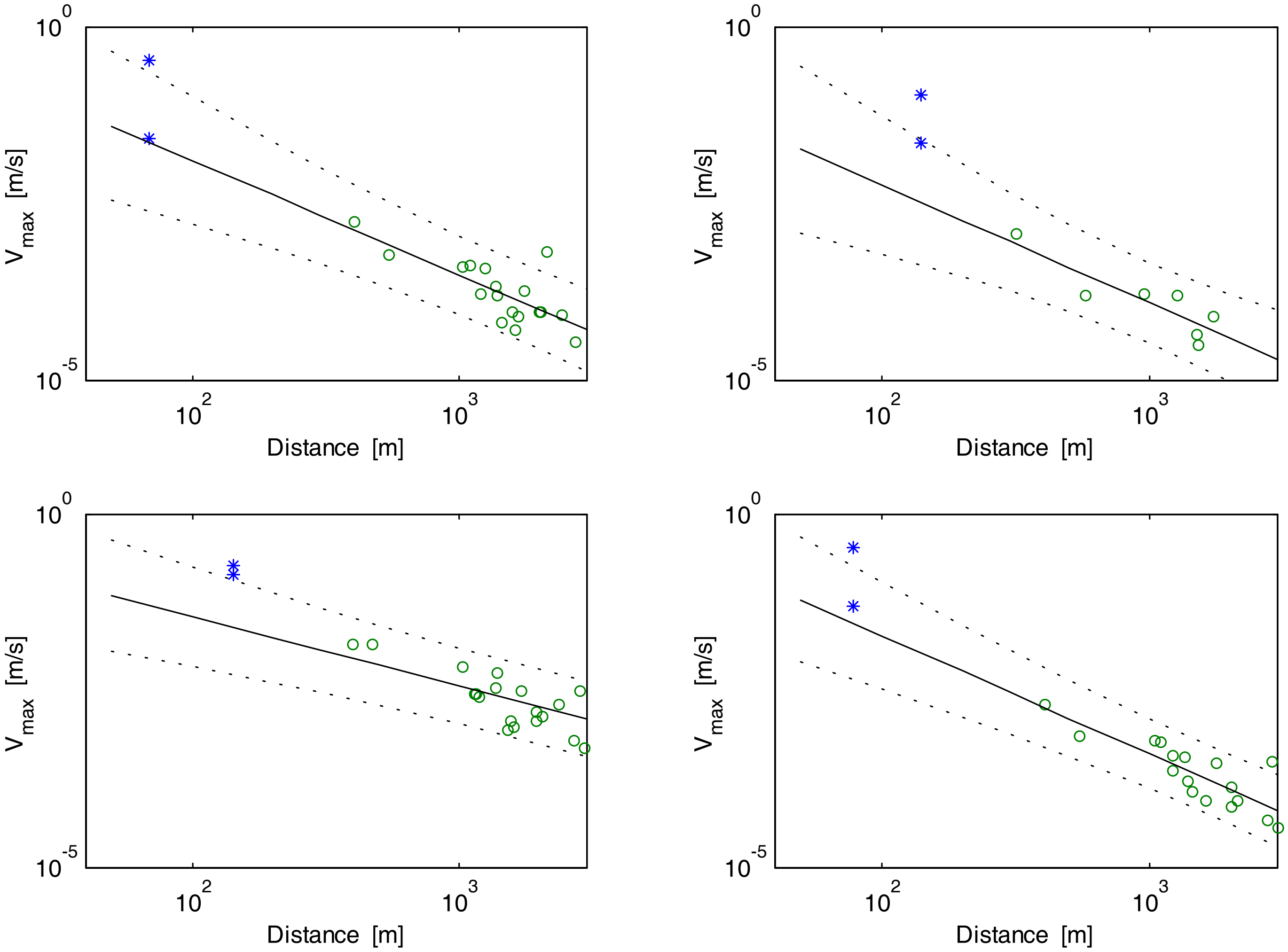

detailed description see Figure 3.1.

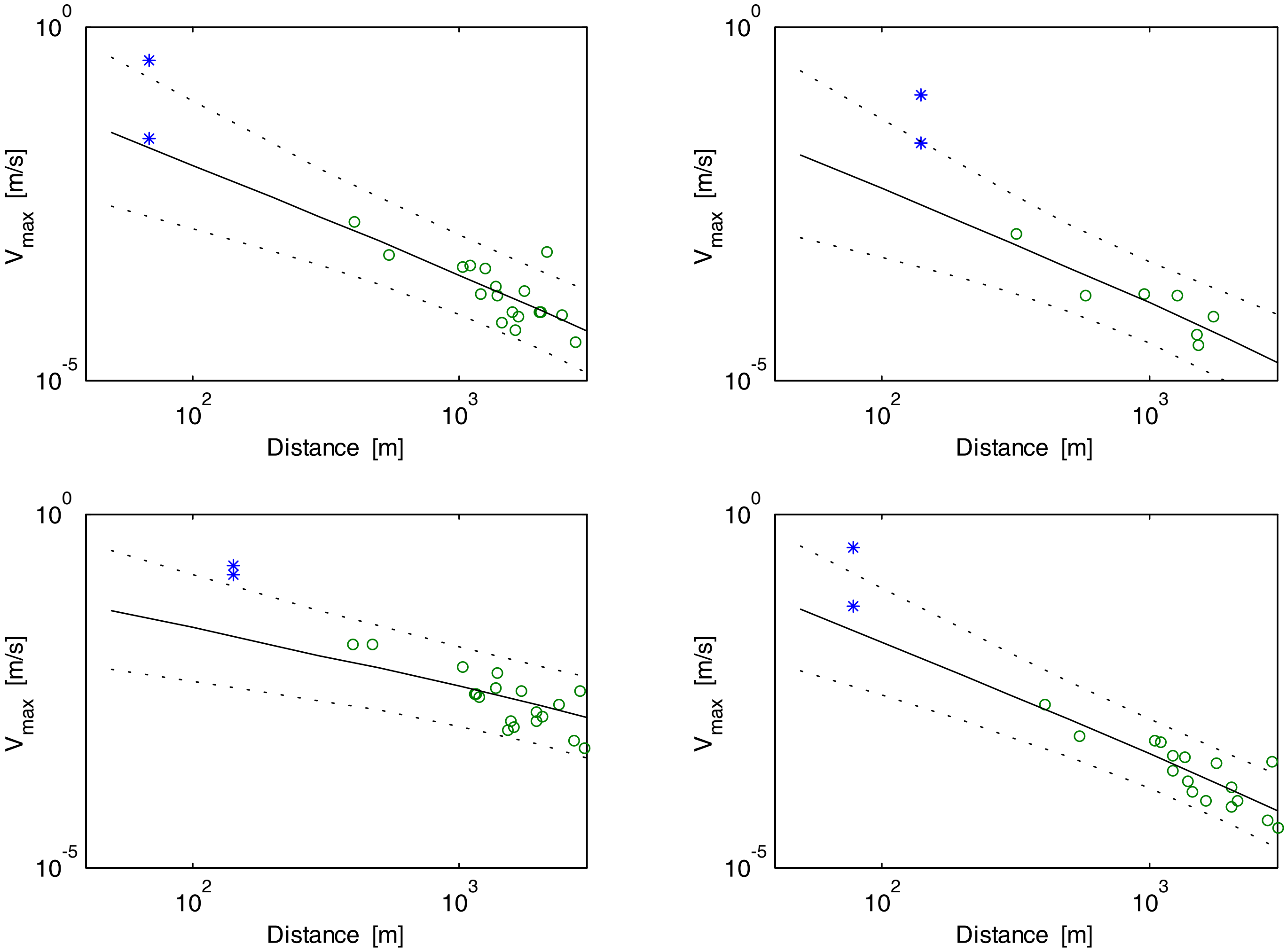

10^0
10^{-5}
V_{max} [m/s]
10^2
10^3
Distance [m]
10^0
10^{-5}
V_{max} [m/s]
10^2
10^3
Distance [m]
10^0
10^{-5}
V_{max} [m/s]
10^2
10^3
Distance [m]
10^0
10^{-5}
V_{max} [m/s]
10^2
10^3
Distance [m]

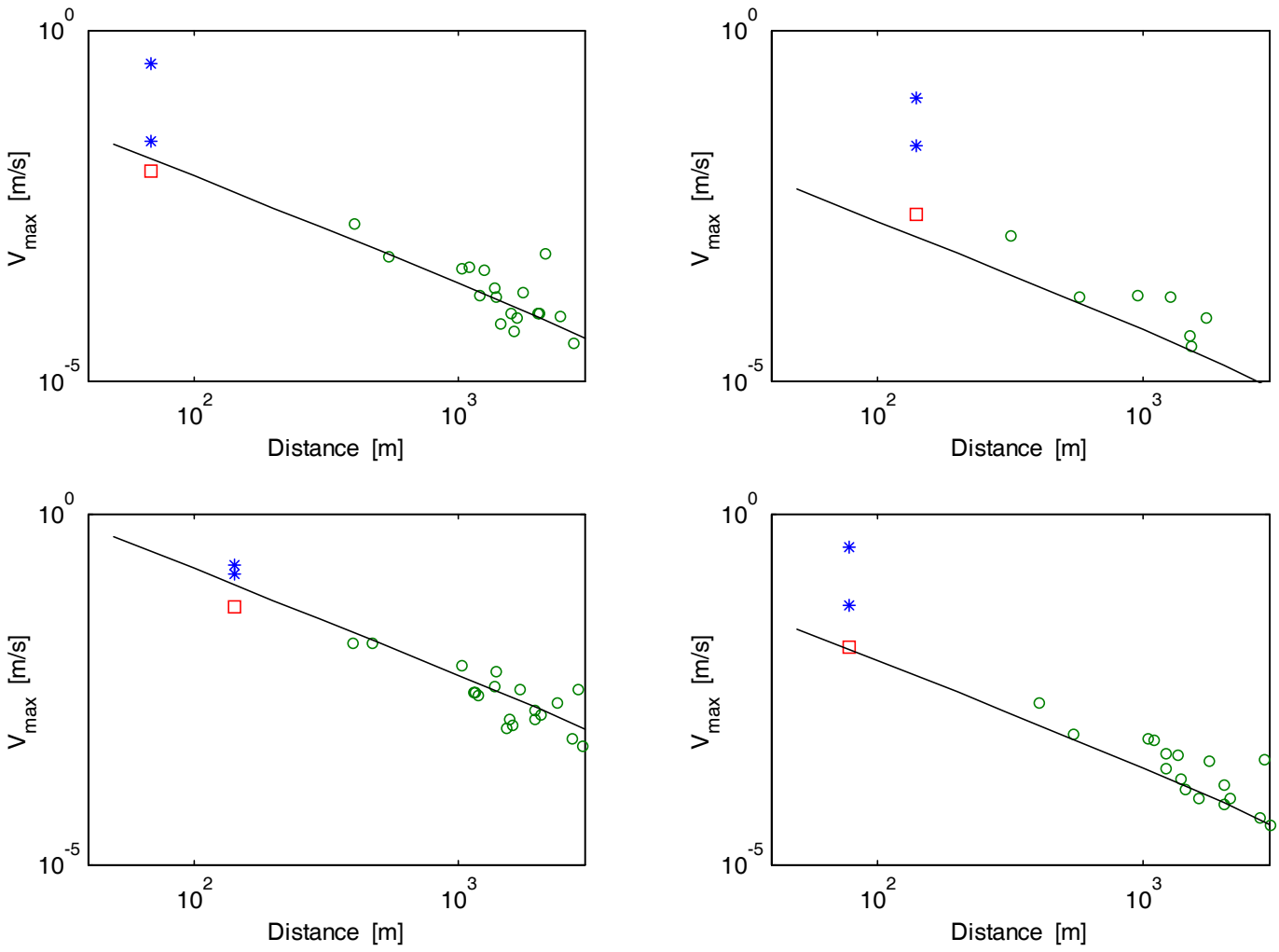

for near field. For a more detailed description see Figure 3.1.

The third attenuation model has features of both previous models. The following equation was used

$$V(R)=\frac{V_o}{R^n}\exp(-\pi f_o R/V_s Q) \quad \textbf{(3)}$$

where f_o is the dominant frequency in signal, Q is the quality factor and V_s is velocity of S-wave. The quality factor was fixed ,Q = 200. The V_o and n were calculated using least square regression. Figure 3.3 shows data and attenuation model given by equation 3. The 'n' is equal to 1.5 for event one, two and four. The V_o correlates well with seismic moments of seismic events. Models 2 and 3 fit data with the same precision (see Figure 3.2 and Figure 3.3).

The final attenuation model (model 4) for far field data is

$$V(R)=\frac{CM_o}{R^{1.5}}\exp(-\pi f_o R/V_s Q) \quad \textbf{(4)}$$

where C= $1/(2*10^{10})$, Q = 200 V_s = 3600m/s.

Figure 3.4 shows the attenuation curve of model 4 developed using only far field data. The square symbol indicates the estimation of the PGV using McGarr's formula (*McGarr*, *1981*), which was developed for application in the near field in solid rock.

$$PGV = \frac{0.57 \Delta \sigma r_o}{\mu R} \quad \textbf{(5)}$$

where r_o is the source radius. Figure 3.4 shows that equation 4 approximates far field attenuation and the near field effect given by equation 5 well.

Finally, it can be concluded, that ground motions of events 1, 2 and 4 (see Table 3.1) have strong amplification factor in the stope. However, a large event with magnitude 2.4 does not show such strong amplification of signal in the stope. Figure 3.4 shows that the model of PGV developed for the far filed fits as well the near field data recorded in the stope. The PGV recorded in the hangingwall and the footwall is almost identical. Therefore, it could be deduced that the stope does not produce amplification of a seismic signal in this case. This observation is important for hazard assessment in stopes.

The characteristics of event ground motion that caused damage are needed to understand how support performed and why it reached failure. Because there are only a few strong motion recordings available, it is very difficult to have the reliable, empirical relationship for the PGV in the near field. Only four events have been used in the final analysis, which is a small data set for this type of analysis. This attenuation relationship needs to be updated as and when more data on strong ground motion is recorded.

4. Standard Spectrum Shape

For support design it is important to understand the frequency band, in which the PGV will occur. For this purpose the Standard Spectrum Shape of the excavation will be calculated.

Further information regarding the ground motion is obtained in the frequency domain. The amplitude spectrum of displacement, velocity or acceleration gives a range of frequencies with the largest energy.

As described in the beginning of the chapter, the amplitude of spectra is controlled by the seismic source, path attenuation and site amplification. Separation of these components gives a good understanding of site specific characteristics. However, if analysis focuses on large events (e.g. radius 50m) recorded in or near the source region (e.g. 80 m), the separation could be ambiguous, as the source could not be approximated using the point source model. Figure 4.1 presents Fourier spectra for different events recorded at the same site in the stope. Under these conditions the geotechnical parameters of the stope should be essentially identical, so the significant difference in the spectra can be attributed to the influence of source mechanism. The figure shows that maximum frequency content lies in a band between 10-100Hz. The larger events have stronger low frequency content and smaller events appear to be relatively richer in high frequency content.

Potential for structural damage increases when there is resonance of the ground. Resonance occurs when the natural frequency of the stope environment is close to the dominant frequency of the incoming signal. Detailed inspection of spectra does not reveal the presence of resonance in the frequency range from 10 Hz to 100 Hz. Therefore, site amplification does not take place in stope environments, within frequency bands controlled by the dominant signal of large seismic events. Previous studies of *Cichowicz et al*. (*1999*) shows strong resonance in the wall of mining excavations of around 400 Hz.

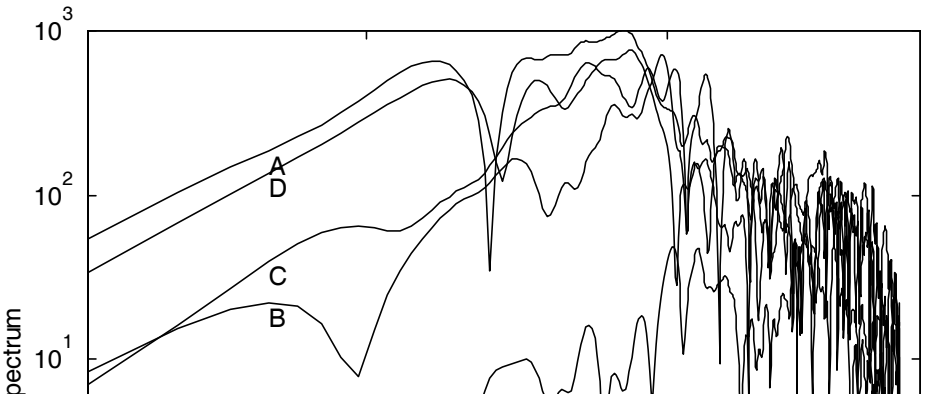

Figure 4.1. Fourier amplitude spectra calculated from accelerograms from the five events:
(A) 25 November 2000, 11:25:22, magnitude 1.2 , distance 69 m;
(B) 11 November 2000, 15:18:31, magnitude 0.7 ,distance 141m;
(C) 4 December 2000, 17:22:58, magnitude 2.4 ,distance 142m;
(D) 7 November 2000, 17:01:27, magnitude 1.2 ,distance 78m;
(E) 27 November 2000, 20:24,weak ground motion .

5. Strong and weak ground motion in footwall and hangingwall

Fortuitously, at one stage of the experiment at Driefontein Mine, a unit with one vertical and two horizontal components recorded a very strong ground motion with peak ground acceleration of 118 m/s^2 and a peak ground velocity of 0.46 m/s (see Figure 5.1). The dominant frequency of these records is less than 30 Hz. It demonstrated that the motion of stope hangingwall could have a horizontal component as strong as the vertical one.

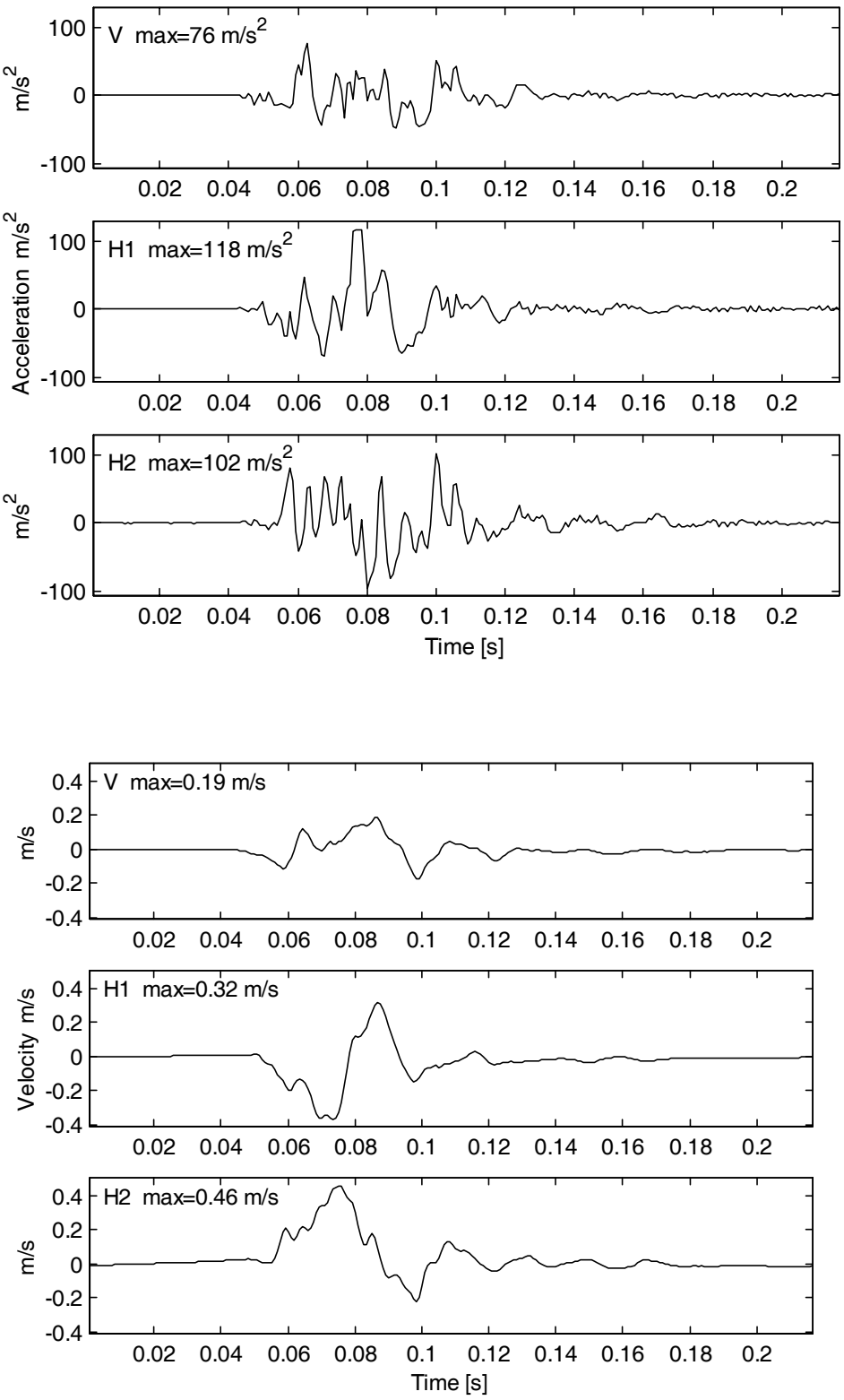

Figure 5.1. Seismic event with magnitude 2 located 87m from strong ground motion sensors, Driefontein Mine, September 29, 2000, 15:34:35. Accelerograms and velocities of vertical (V) and two horizontal (H1, H2) components are the largest strong ground motions recorded during the course of the project (PGA= 118 m/s ^{2}, PGV= 0.46m/s).

The distance between the hangingwall and footwall is relatively small compared to the distance between the seismic source and the positions of the sensors. Therefore, the observed difference in the waveform of ground motion recorded at the hangingwall and footwall are controlled by stope geotechnical parameters such as length, height, distance to face and physical parameters of quartzite and lava. It is expected that waves with a wavelength much longer than the length of the stope are passing through the stope without any disturbance. For example, for a stope of length 50-100 m a signal below 10 Hz (wavelength longer than 360m) will be undisturbed. A wave with a high frequency will be significantly affected by the presence of free space between the hangingwall and footwall, and the effects of attenuation, reflection, refraction and scattering will be observed. Note that a large seismic source produces a broad band signal with low and high frequency components.

The terms "strong ground motion" and "weak ground motion" are used to classify observed records. In this report strong ground motion is used to describe seismograms characterised by few oscillations and a dominant pulse with a strong component of low frequency. The spectrum of strong ground motion is usually broad band, so a high frequency signal is present as well. Seismograms described in this way are the near-field records, where the distance between seismic source and sensors is small. Weak ground motions have, by definition, a smaller signal amplitude than strong ground motion. For small seismic sources the weak ground motion has a strong component of high frequency, however for large seismic events located far from the sensor, the weak ground motion is reached in the low frequency.

Figures 5.2 to 5.7 show examples of ground motion recorded at the hangingwall (H) and footwall (F). The velocity and the displacement are calculated by the integration of acceleration of ground motion. Appendix 2 presents details of the method.

Seismograms displayed in Figures 5.2, 5.3, 5.4, 5.6 and 5.7 are near-field strong ground motions with large values of PGA and PGV. Accelerograms of the strong ground motion at the hangingwall and footwall have some similarity, the major phases can be identified on both records. The velocity and displacement of the ground motion have more common features. All these events cause permanent deformation of the hangingwall or footwall (see Figure 5.7). When the source is located below the stope the stronger deformation is in the footwall, as is expected. A strong event with magnitude 2.4 was located above the stope (see Figure 5.4). This event caused strong motion in the hangingwall and footwall. The database consists mostly of records of events located below the stope, so it is difficult to explain the footwall behaviour during the magnitude 2.4 event.

Figure 5.5 shows acceleration of the weak ground motion with a strong contribution of high frequency. The weak ground motion reveals a total lack of coherence between ground motions in the hangingwall and footwall, i.e. the major impulses are not in phase at all. In most cases, ground motions at the hangingwall and footwall are not alike. The records of weak ground motion dominate the available databases of in-stope ground motion measurements. Such data is mostly useless, as it does not carry information about damaging ground motion. Weak ground motion causes support response only in its elastic range and provides no information about what happens in a range of plastic deformations. Collected records reveal that the support response to strong ground motion is essentially different to the support response to weak ground motion.

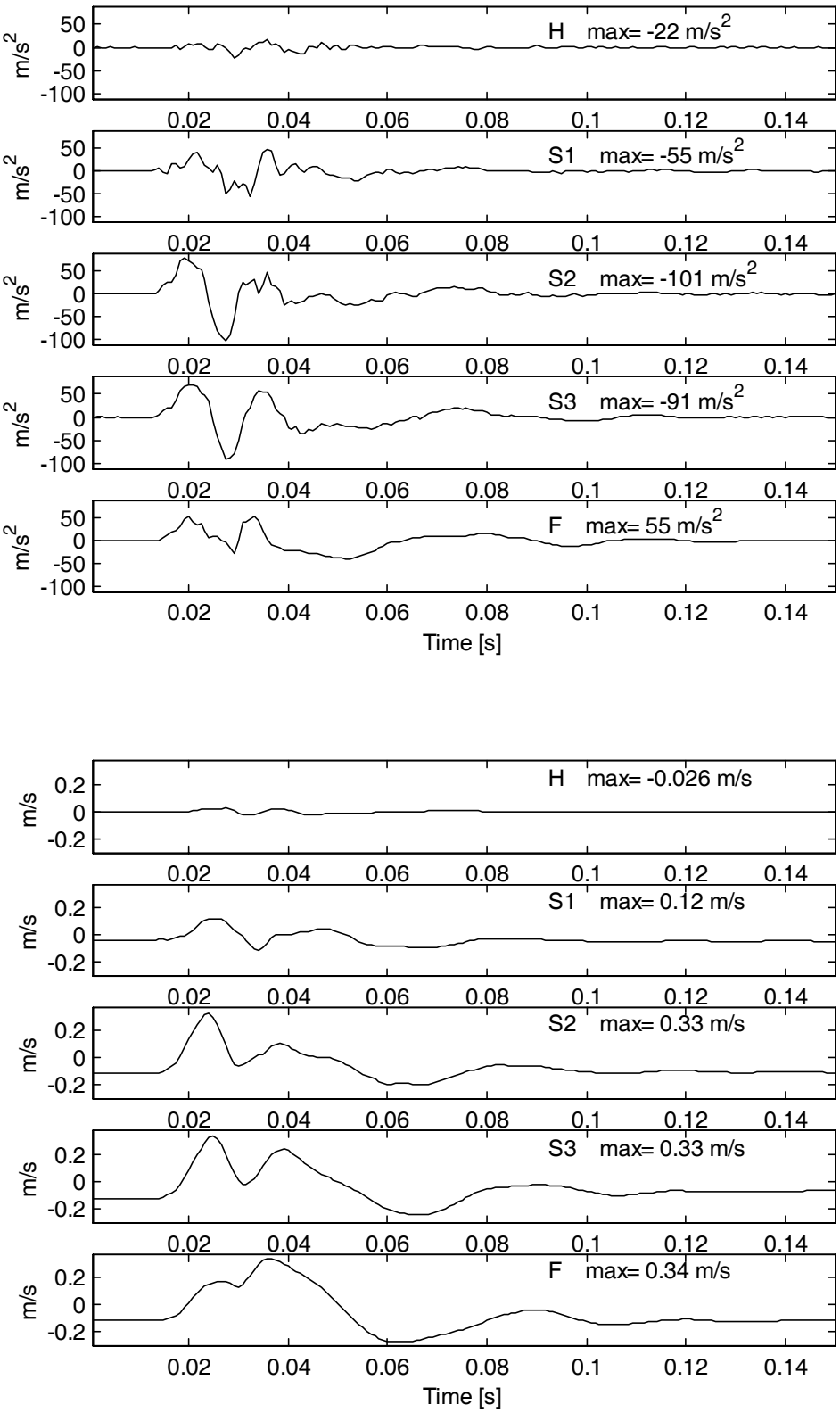

Figure 5.2. Seismic event with magnitude 1.2 located below the stope, 69m from strong ground motion sensors, Mponeng Mine, November 25, 2000, 11:25:22. Hangingwall (H), support (S1,S2,S3), and footwall (F).

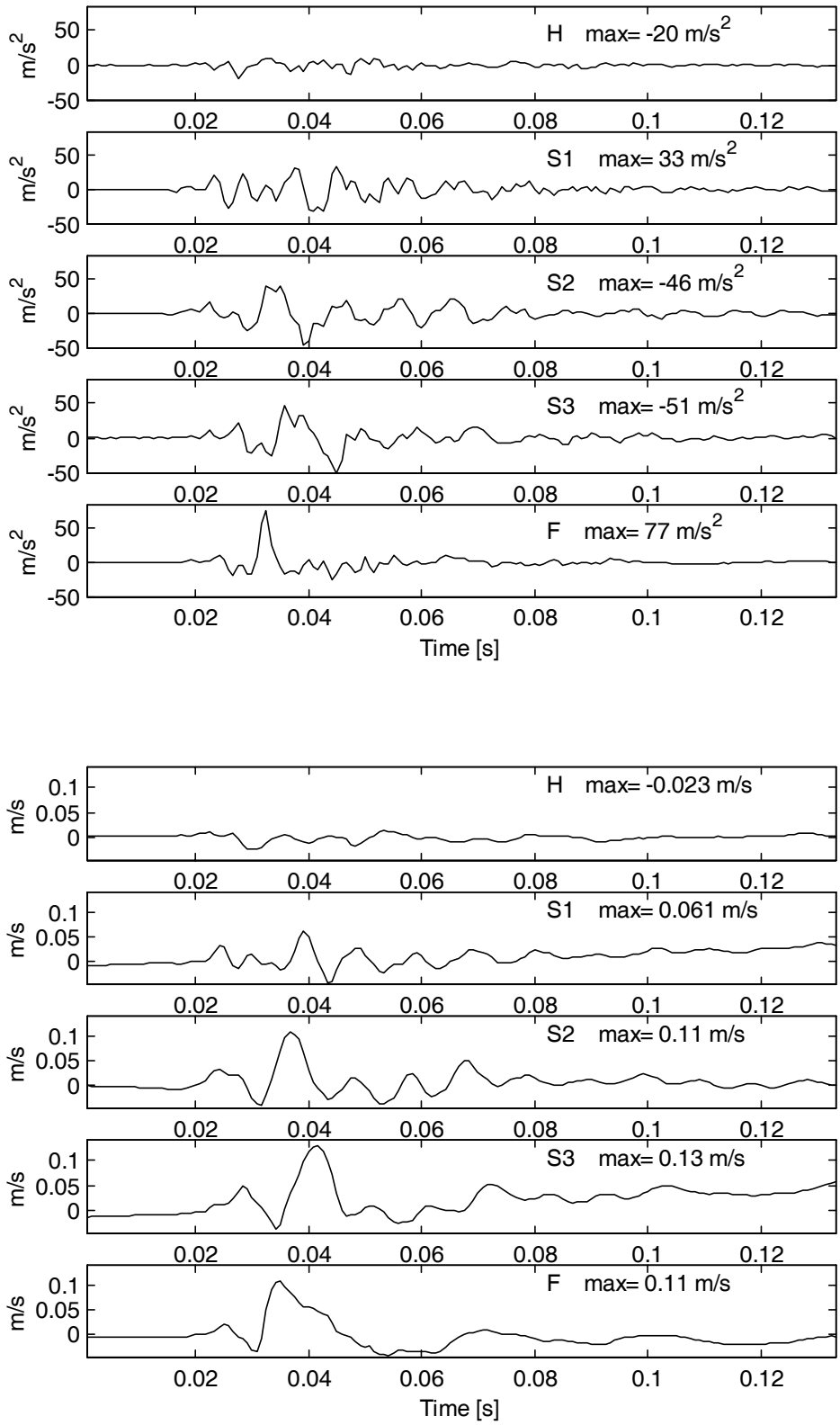

Figure 5.3. Seismic event with magnitude 0.7 located below the stope, 141m from strong ground motion sensors, Mponeng Mine, November 11, 2000, 15:18:31. Hangingwall (H), support (S1,S2,S3), and footwall (F).

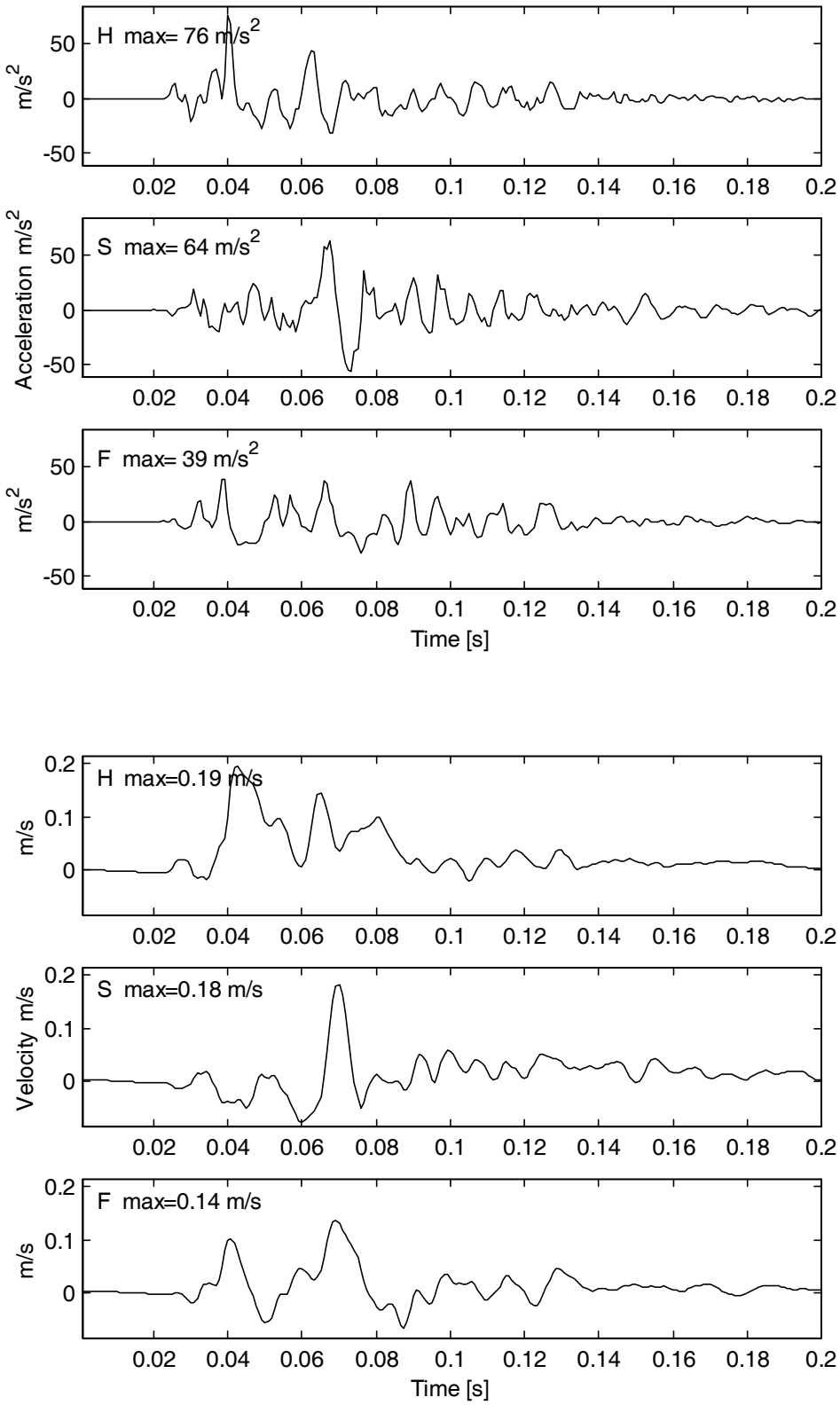

Figure 5.4. Seismic event with magnitude 2.4 located above the stope, 142m from strong ground motion sensors, Mponeng Mine, December 4, 2000, 17:22:58. Hangingwall (H), support (S), and footwall (F).

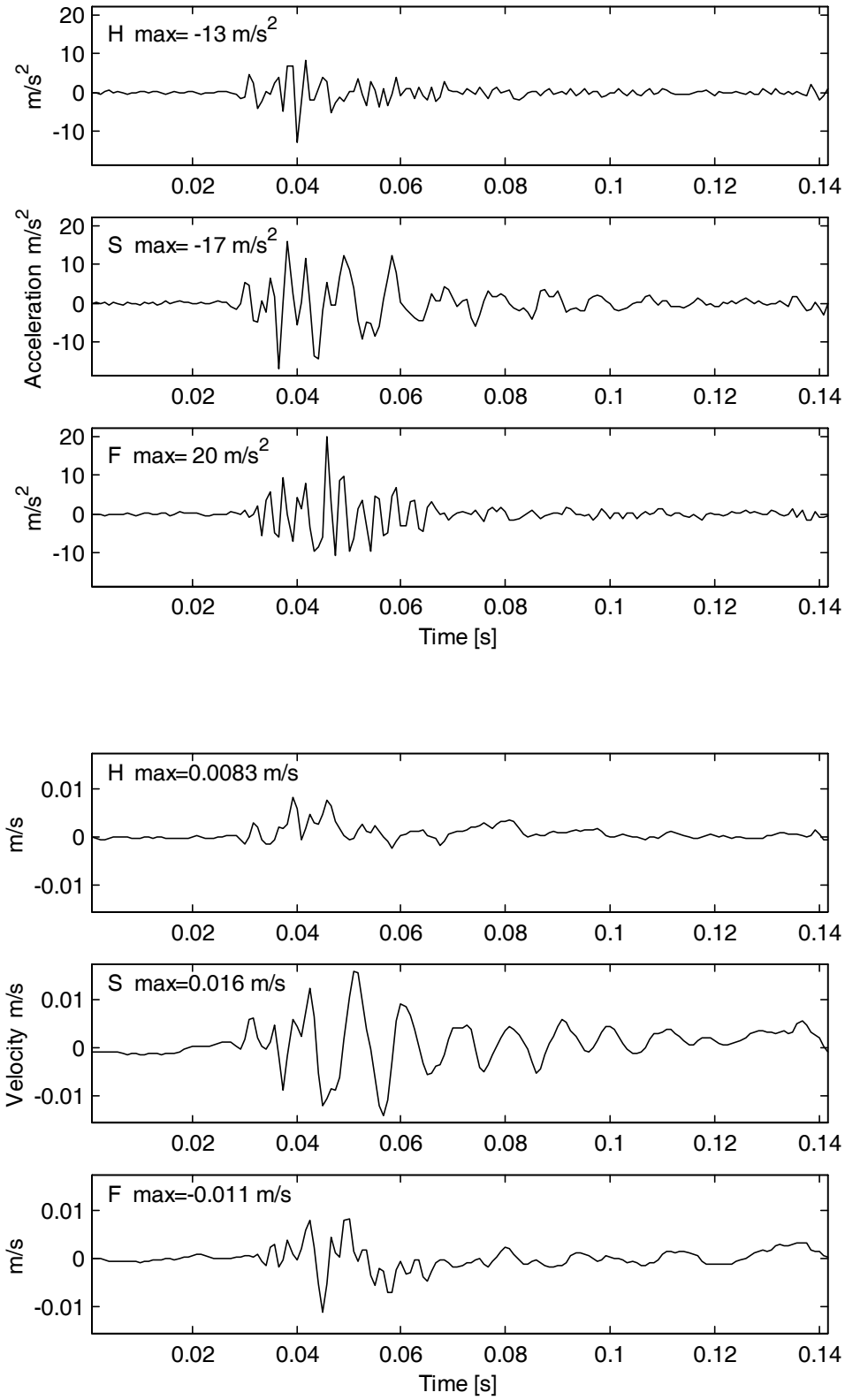

Figure 5.5. Weak ground motion. Seismic event with magnitude 0.5 located 79 m from sensors, Mponeng Mine, December 8, 2000, 15:23:03. Hangingwall (H), support (S or S1, S2, S3), and footwall (F).

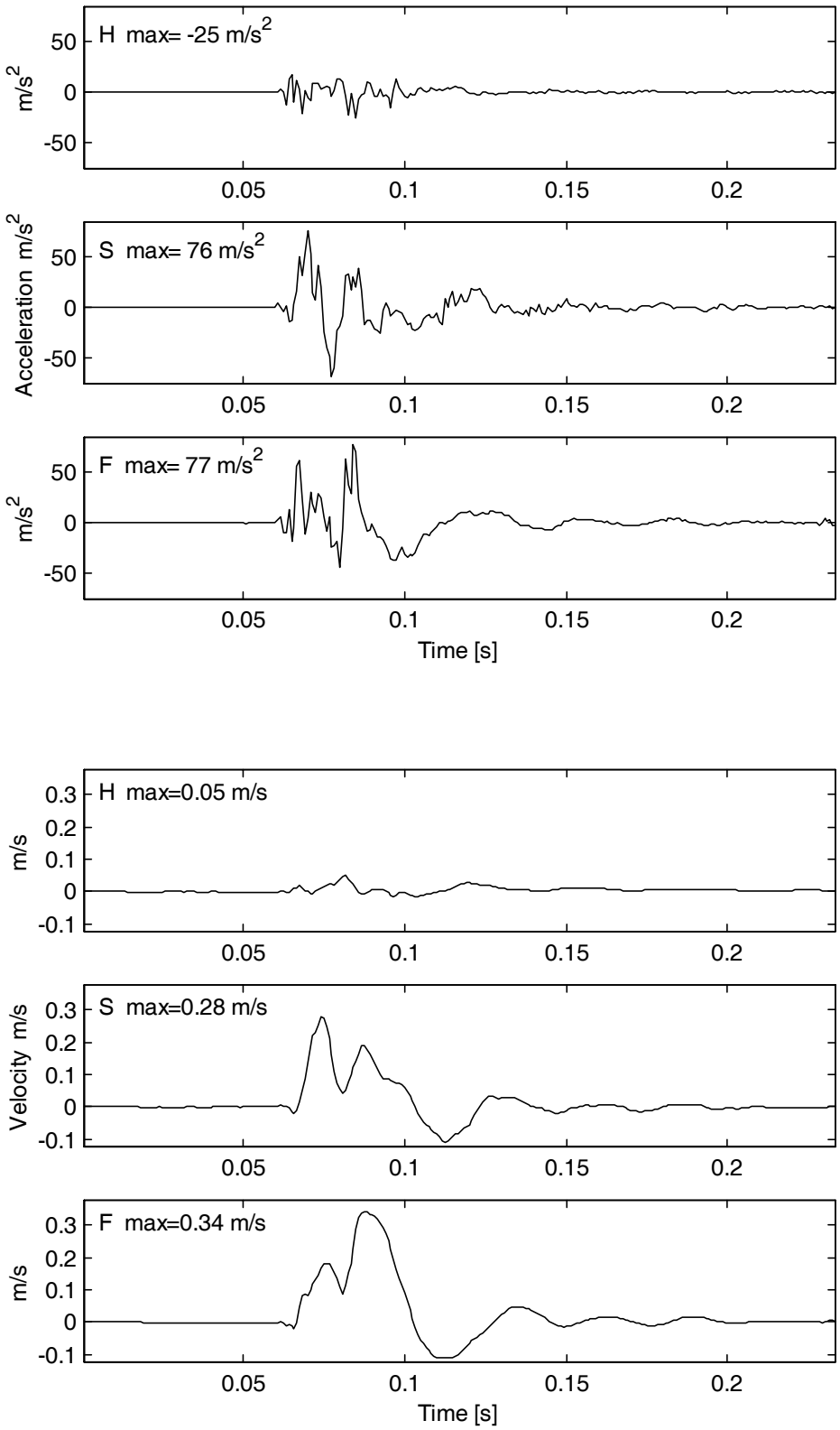

Figure 5.6. Strong ground motion. Seismic event with magnitude 1.2 located 78 m from sensors, Mponeng Mine, November 7, 2000, 17:01:27. Hangingwall (H), support (S), and footwall (F).

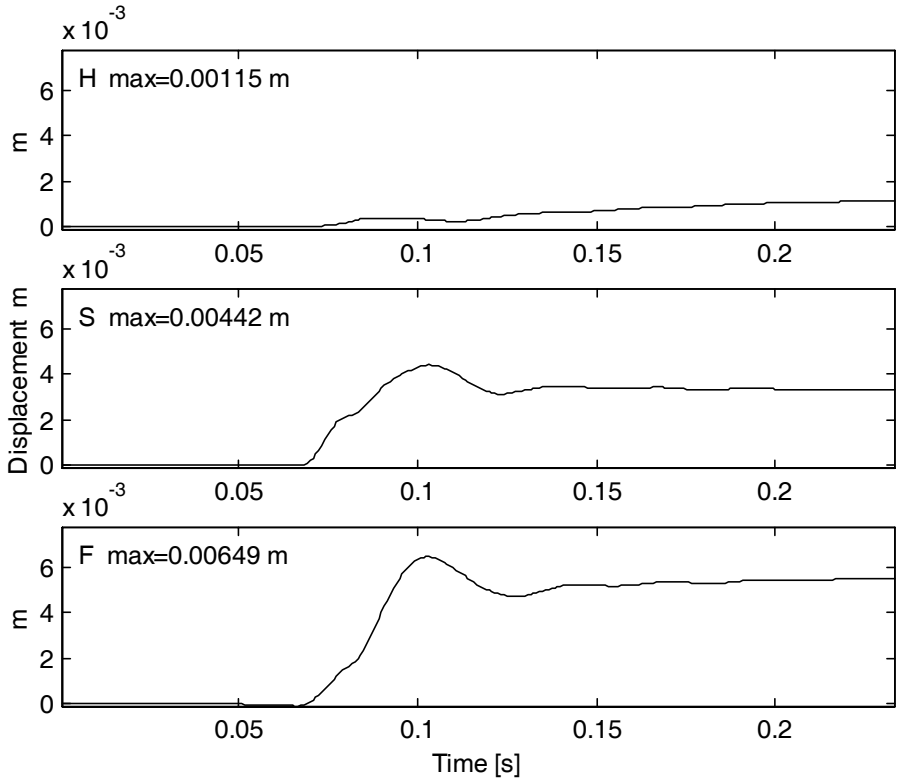

Figure 5.7. Displacement of strong ground motion; seismic event with magnitude 1.2 located 78 m from sensors, Mponeng Mine, November 7, 2000, 17:01:27. Hangingwall (H), support (S), and footwall (F).

6. Support (brick composite pack) response to seismic load

Concluding from the previous chapter, the support units have been exposed to two major forces. One is applied from the hangingwall and another from the footwall. In the observations, these forces have never had the same amplitude.

An experiment was conducted to monitor the motion of support (brick composite pack) under a seismic load. To achieve this, one vertical accelerometer was installed in the pack. After very encouraging results, obtained from the measurements of middle support movement under seismic load, several questions arose. How representative could one measurement in the support be? What is the relative movement of different parts of the support? To answer these questions three vertical sensors were placed in the brick composite pack. This arrangement was only temporary.

Figures 5.2 to 5.7 display the motion of the support at one or three points. The figures show acceleration, velocity and displacement (only Figure 5.7) of ground motion in the footwall (F), motion of the support (S or S1 S2 S3) and ground motion in the hangingwall (H). For a seismic event located below the stope, it is clear that the strong ground motion from the footwall is passed to the first and to the second accelerometers in the pack, almost without significant distortion. The pattern of velocity in the footwall and in the middle of the support is very similar in shape and amplitude, however the velocity in the upper part of the support is much smaller. At this stage one thing is clear - a pack is not moving as one uniform block. The difference in ground motion in the hangingwall and footwall has an effect on how the pack is deformed.

Velocity of motion in the support caused by an event located above the stope is shown in Figure 5.4. A strong signal is clearly coming from the top. However, the ground motion in the footwall is strong as well.

Lastly, Figure 5.5 shows weak ground motion caused by a seismic event located below the stope. A pattern of support motion caused by weak ground motion is not as clear as it is for strong ground motion. Therefore parameters of weak ground motion cannot be used as an indicator of the support's behavior under strong ground motion.

Most of the support motion closely follows ground motion. The similarity of these motions is observed up to 70-100 m/s^2. This similarity reflects the fact that the support, under a dynamic load of seismic ground motion, behaves as an elastic, or almost elastic, material. The left hand side of Figure 6.1 shows acceleration versus support displacement in the hangingwall (top) and the footwall (bottom). The value of acceleration is proportional to the applied load. If one multiplies 70-100 m/s^2 by the assumed mass of a loose rock, one can calculate the force acting on the support. The height of block supported by support is 1.8m (see radar measurement Appendix 3).

A seismic event of magnitude 1.2, that caused strong ground motion, with peak ground velocity of 0.34 m/s, was located in the footwall 78m from the sensors. It is clear that the applied seismic load occurred as a series of two impulses and each of them caused a displacement of 2mm, with a final displacement of about 4.5 mm (see Figure 6.1).

Amplitudes of applied forces from the hangingwall and footwall are not equal. Graphs on the right of Figure 6.1 show the relative displacement of the support and the hangingwall (top) or footwall (bottom). It is clear that the movement of the bottom of the support is in phase with the footwall, however the movement of the support versus the movement of the hangingwall is not in phase.

Figure 6.2 shows that weak ground motion caused unsynchronised motion of the support. The amplitude of the support motion is low and has a chaotic character.

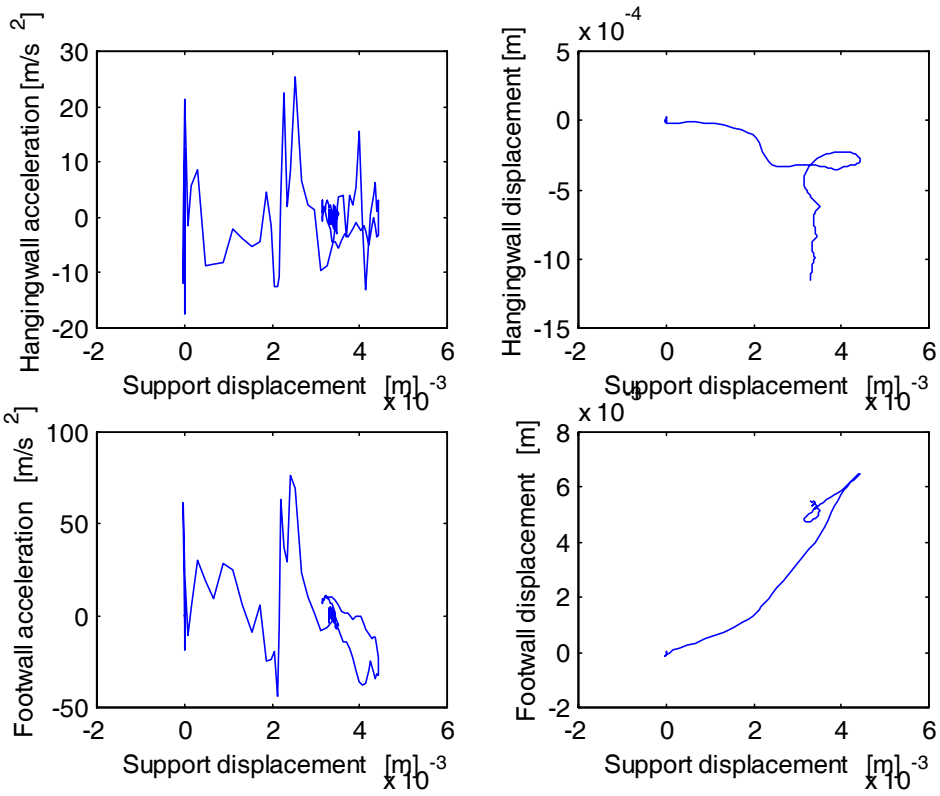

Figure 6.1. Seismic sensors were placed in the hangingwall, the support and the footwall. A seismic event, of magnitude 1.2, that caused strong ground motion, with peak ground velocity of 0.34 m/s, was located in the footwall 78m from the sensors. Figures on the left show acceleration versus support displacement in the hangingwall (top) and the footwall (bottom). The value of acceleration is proportional to the applied load. It is clear that the applied seismic load occurred as a series of two impulses and each of them caused a displacement of 2mm, with a final displacement of about 4.5 mm. Amplitudes of applied forces from the hangingwall and footwall are not equal (note the scale on the acceleration axis). Figures on the right show the relative displacement of the support and hangingwall (top) or footwall (bottom). It is clear that the movement of the bottom of the support is in phase with the footwall, however the movement of the support versus the movement of the hangingwall is not in phase. This means that the damage caused by the seismic event happened in the upper part of the support.

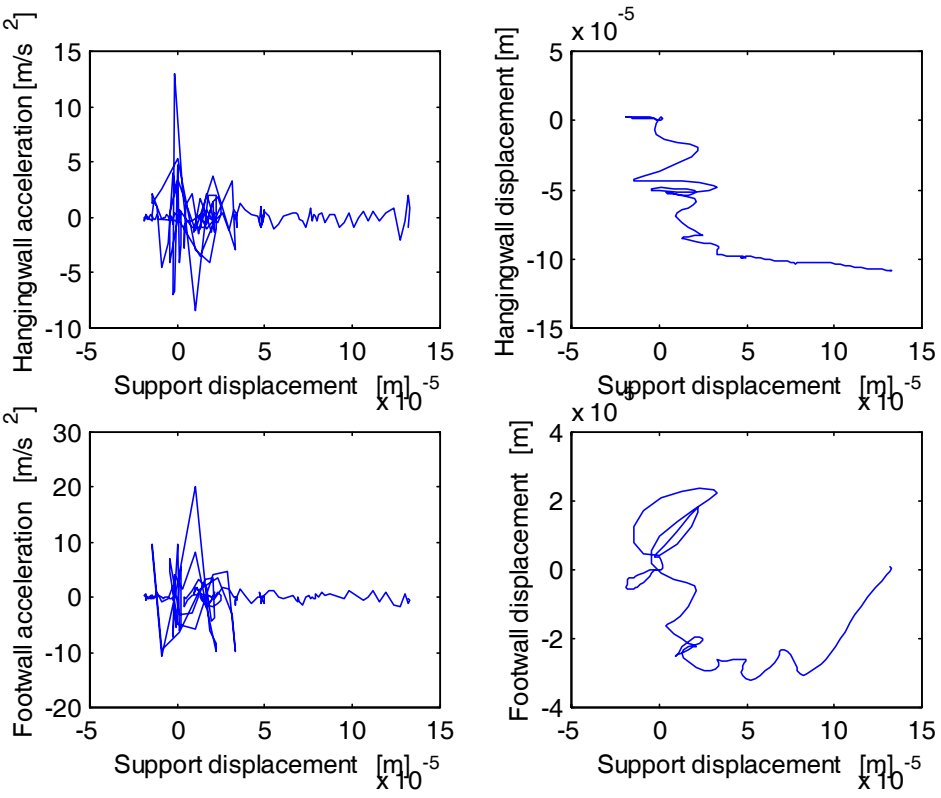

Figure 6.2. A seismic event with magnitude 0.5 located 79m from strong ground motion sensors, Mponeng Mine. Weak ground motion of the seismic event is located above the stope. For details see Figure 6.1. Note that the displacements are two orders of magnitude smaller than in the case of Figure 6.1.

7. Discussion

7.1. Could PGV or PGA be used as a measurement of damage in support?

The PGV or PGA is the popular index for assessing damaging ground motion in structures. These parameters are most often used in the engineering analysis for the characterization of seismic hazard. It is a single value indicator which is relatively easy to determine, but which often leads to incorrect seismic risk estimation. In fact, the peak values alone cannot describe adequately all the effects associated with the ground shaking since the frequency content and the duration of a seismic wave can play a decisive role.

PGV and PGA (converted to PGV), are not the best parameters for measuring the input energy to support. Specifically, they should not be used at this stage of research when one is trying to understand what happens in the support during seismic loading. The full waveform should be studied instead. For example, in data that has been analysed, damage happened as a result of two strong impulses and each one caused a displacement of 2mm. Therefore, using only the PGV parameter, the error in the estimation of displacement in the stope would be 100%!

7.2. Is the limit of 3m/s in support designs just right?

The highest values of the PGA and the PGV monitored so far are in the range 77-118m/s^2 and 0.34-0.46 m/s respectively. These parameters of strong ground motion were caused by seismic events of magnitude 1.2-2.4 observed from distances 80-140m. The collected data clearly show that magnitude and distance are not the only dominant parameters that control properties of strong ground motion. An

event with magnitude 0.9 recorded at 124 m from source has PGA =34 m/s^2. These ground motions have characteristics of the near field such as one or two strong oscillations with a relatively low frequency of 10-30Hz. The near field ground motion usually causes damage, as in our observation, however permanent deformation of the stope is not extensive, only a few millimeters. Data indicates that the movements of the stope caused the support response to exceed a level of recovery deformation.

The observed peaks are far below the 3m/s used in current support designs as a maximum expected velocity. Thus far we have not observed a large seismic event, with a magnitude of 2.5-3.0, recorded from a distance of less than 50 m (i.e. a case when a seismic sensor is in the source area). Perhaps that type of record would give a different conclusion.

Near field features of ground motion have been observed with permanent deformation in the stope and in the support, but still very far away from the critical value of 3m/s. The documentation has been investigated that was used as the base for defining 3m/s as the design parameter. However, all the evidence suggests that the value was purely speculative.

7.3. Support under cyclic loading

The Handbook on Rock Engineering Practice for Tabular Hard Rock Mines, follows Wagner's equation (*Wagner*, *1984*), that states, that seismic input energy has to be absorbed by support. The capacity of support to absorb energy is equal to the area under a load-displacement curve (see Figure 7.1A). This relationship correctly estimates a maximum possible displacement of support during a seismic event. However, it is not suitable to estimate energy absorbed by support under a seismic loading, as claimed. The source of confusion starts when ground motion caused by a seismic event is understood as a monotonic dynamic load so that it can be modelled, for example, using an experiment with a press. Seismic ground motion has a cyclical behaviour. This phenomenon comes as no surprise, although it is not considered by Wagner's equation.

However, the cyclical response of the support (brick composite pack) to cyclic seismic loading was unexpected. Observed vibrations of the support suggests that some portion of impacted energy into the support will be returned to the surrounding rock. This means, that the entire input energy is not being converted to permanent deformation. Therefore the area under a load-deformation curve, calculated from zero to a value of maximum vertical displacement, does not measure the energy absorbed by support, because most of the input energy is returned to the surrounding rock. Energy absorbed by the support is mostly hysteretic energy. This statement has a very practical implication hence it has to be verified by more data.

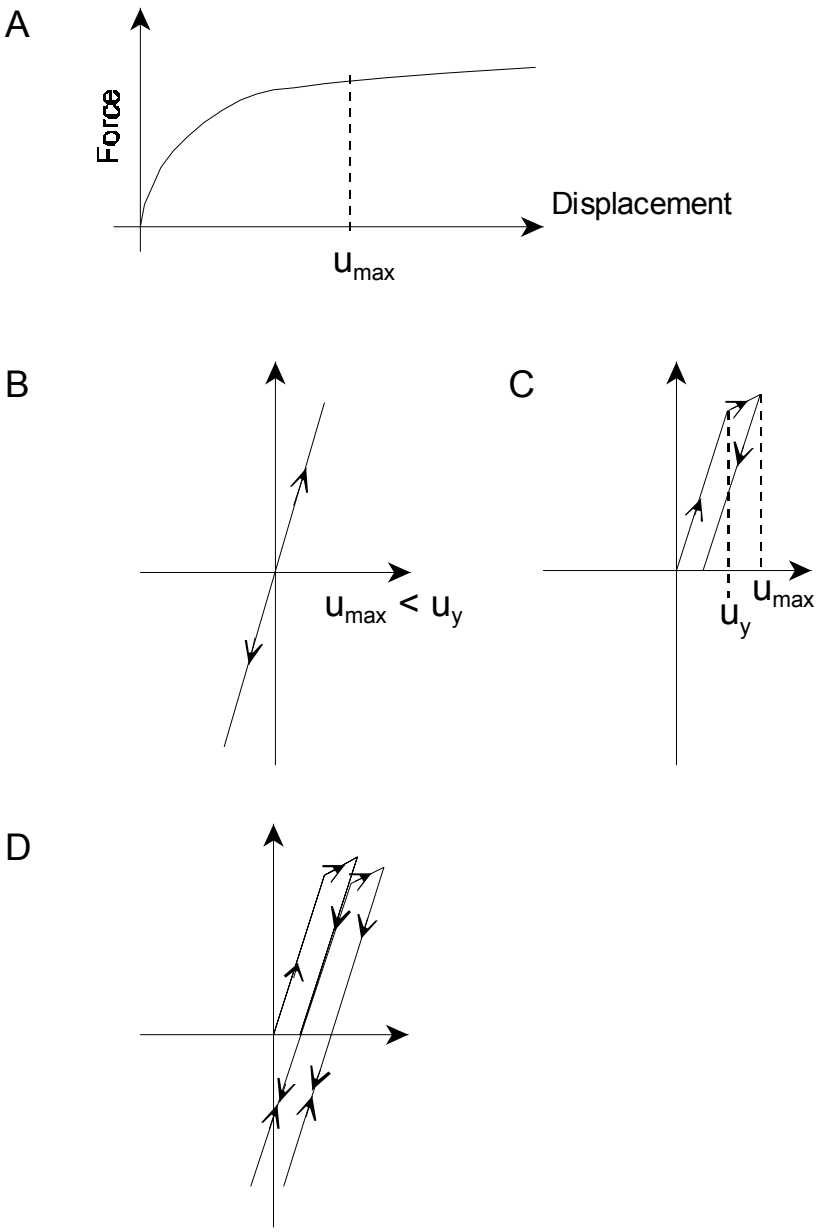

Figure 7.1. (A) Graph shows schematics load deformation relationship during monotonous loading. (B) Elastic system, whether linear or nonlinear, has a force-deformation curve symmetric about the origin. This is a model of recoverable deformation of support under weak cyclic loading. (C) Graph shows the hysteretic model for half cycle, where U_{max} is the maximum displacement and U_y is the yield displacement. A hysteretic relationship is based on the bilinear curve. (D) This is a likely model of unrecoverable deformation of support under near field strong ground motion.

The weak ground motion causes mostly an elastic response of the support (see Figure 7.1B). Support response monitored at three different points shows that the features of support motion are not coherent. Lack of coherency could be caused by a strong high frequency component in the weak ground motion.

After studying a number of examples of the support response to near field strong ground motion, a model of support can be formulated. The brick composite pack can be seen as an ensemble of elasto-plastic elements (Figure 7.1C). The elasto-plastic element absorbs energy (hysteretic energy) during each full cycle of load. The elasto-plastic deteriorating element has unrecoverable deformation when the

displacement reaches a critical value. Hypothetically, the force-deformation curve for two cycles could take the shapes shown schematically in Figure 7.1D).

This is a preliminary model of support response. The exact model of support response can be predicted using a system identification method. To obtain such a model two real seismograms are used: an input signal, which is a seismogram recorded in the hangingwall or footwall and an output signal, which is a seismogram recorded in the support. System identification methods calculate parameters of a force-deformation curve for each cycle of the input signal in order to predict support response (output signal).

7.4. Indexes of damage - further research

In earthquake engineering practice, a nonlinear structure's response characteristics are proposed as damage indexes. The most common parameters are ductility demand and hysteretic energy demand. Ductility demand is the ratio of the peak displacement of a structure to its yield displacement, μ. The hysteretic energy dissipated by an inelastic structure measures cumulative damage by including loading history. The index of hysteretic energy demand is defined as the ratio of hysteretic energy to the elastic stain energy.

A Handbook on Rock Engineering Practice for Tabular Hardrock Mines uses maximum deformation, U_{max}, as the damage index, which is similar to ductility demand. However, true ductility demand normalises a maximum deformation by dividing it by maximal elastic displacement U_y. The normalisation has the advantage that it will allow a comparison of all types of support with each other. For example, in a concrete structure μ= 2 corresponds to the minor damage and μ=4 corresponds to significant damage.

To date it seems that damage hysteretic energy has not yet been calculated for support. The maximum permissible displacement in support lacks a quantifiable consideration of the full seismic inelastic cycle response. As an alternative, the energy based design method can alleviate this shortcoming. Future research has to concentrate on addressing the energy balance for elasto-plastic support material. An energy balance has to be used, that in a proper way describes seismic input energy imparted to support and the contribution of each component of energy has to be estimated.

The indexes have advantages and disadvantages. Ductility demand is, for example, unable to distinguish between a single inelastic deflection and a more damaging sequence of yield reversals. The index of hysteretic energy has an advantage over ductility as a measure of cumulative damage, since it sums the contribution from successive yield cycles, while ductility simply measures the peak displacement. Nevertheless, hysteretic energy demand is unable to distinguish between a sequence of low-amplitude yield cycles and a more damaging single deflection with high-amplitude with the same total energy. Several authors have proposed an index that includes both ductility and hysteretic energy.

Response spectra form another very important group of characteristics of a nonlinear structure. Damage potential is based on analysis of the response of a nonlinear oscillator. Structure that vibrates as a result of applying external forces can be modelled using a nonlinear oscillator. The strong point of response spectra is that they are sensitive to different types of input ground motions. Two major types of strong ground motion can be distinguished: long strong ground motion with several cycles and short strong ground motion with one or two full cycles. The response spectra are complementary to displacement-based design methods because the response spectra calculate maximal displacement (or velocity) as a function of frequency.

7.5. Dynamic response of support due to seismic load - further research

Several issues have to be addressed in further research:

- Monitoring and explanation of relative motion in different parts of the support under strong ground motion in the hangingwall and footwall.
- Estimation of energy that is recovered during one full cycle of support oscillation, i.e. the portion of imparted energy that is returned to the rock without damaging the support.

- Estimation of the hysteretic and damping energy of the support for different ground motion.
- Attempt to introduce damage indexes (well known in the field of earthquake engineering) that include maximum permissible displacement, hysteretic energy and response spectra.

Generally, knowledge that will allow prediction of support response caused by a known ground motion of the footwall and hangingwall has to be acquired. The ultimate goal of the research is to set parameters for the design of support that will control energy distributed per cycle of deformation.

8. Conclusion

The parameters of strongest ground motion observed so far are:

- PGA = 77- 118 m/s^2, PGV = 0.3-0.46 m/s at frequency f = 10-30 Hz. These parameters of strong ground motion are caused by seismic events of magnitude 1.2-2.4 observed from distances 80-140m.
- An attenuation model of peak ground velocity is proposed to predict ground motion of future seismic events.
- Ground motion of moderate seismic events with magnitude 0.7 and 1.2 is amplified in the stope. However, ground motion generated by a large seismic event with magnitude 2.4 is not amplified in the stope. This statement is based on three independent estimations.

- Ground motion at footwall and hangingwall have similar features, however for weak or high frequency, signals are not coherent.
- The support is subjected to the combined action of both vertical and lateral loads. The amplitude of lateral ground motion is of the same order as vertical ground motion.
- The monotonous loading (load deformation) curve does not adequately describe support motion under seismic load. The cyclic loading model has to be used to predict support response.
- The observed vibrations of support suggests that some portion of impacted energy into the support will be returned to the surrounding rock. This means that the entire input energy is not being converted to permanent deformation.
- One support unit studied (brick composite pack) does not move as one uniform block. The difference in ground motion of the hangingwall and footwall has an effect on how the pack is deformed.
- It is evident that the demand imposed on the support by strong ground motion is different to that imposed by weak ground motion. Therefore, parameters of weak ground motion cannot be used as an indicator of support behavior under strong ground motion as they are quantitatively different, a simple scaling law is not applicable. Weak ground motion causes support response only in its elastic range and provides no information about what happens in a range of plastic deformations.

References

Atkinson G. 1984. Attenuation of strong ground motion in Canada from a random vibration approach, *Bull Seism. Soc Am*. 74, p2629-2653.

Butler, A.G. and G van Aswegen. 1993. Ground velocity relationship based on a large sample of underground measurements in two South African mining regions. (*In:* Rockbursts and Seismicity in Mines, Kingston, Ontario, Canada. Rotterdam: Balkema, pp41-51.)

Campbell, K. W., 1985. Strong motion attenuation relations: a ten years perspective, *Earthq. Spectra*, 1, pp759-804.

Cichowicz, A., Milev A.M. and Durrheim, R. J. 1999. Transfer function for a seismic signal recorded in solid rock and on the skin of an excavation. *Journal of South Africa Institute for Mining and Metallurgy*, July/August, p201-206.

Cichowicz, A., Milev A. M. and Durrheim, R. J. 2000. Rock mass behaviour under seismic loading in deep mines environment. *Journal of South Africa Institute for Mining and Metallurgy*, March/April, pp121-128.

Cichowicz, A. and R.W.E Green. 1989. Changes in the early part of the seismic coda due to localised scatterers: The estimation of Q in a stope environment. *Pure and Appl. Geophys*, 129, 193, 208.

Cichowicz A., R.W.E Green, and A. van Zyl Brink. 1988. Coda polarisation properties of high-frequency micro seismic events, *Bulletin of the Seismological Society of America*, vol. 78, No 3, pp. 1297-1318

Jager A. J. and Ryder J. A. 1999. A handbook on rock engineering practice for tabular hard rock mines. Safety in Mines Research Advisory Committee (SIMRAC), Johannesburg. Cape Town: Creda Communications.

Linkov, A. M., and R.J. Durrheim. 1998. Velocity amplification considered as a phenomenon of elastic energy release due to softening. (*In: Rossmanith. Mechanics of Jointed and Faulted Rock.* Rotterdam: Balkema, pp.243-247)

McGarr, A. 1981. Analysis of peak ground motion in terms of a model of inhomogeneous faulting. *Journal of Geophysical Research*, 86, page 3901-3912.

McGuire, R. K., and T. C. Hanks. 1980. RMS accelerations and spectral amplitudes of strong ground motion during the San Fernando, California, earthquake, Bull Seism. Soc. Am, 70, p1907-1919.

Ortlepp, W. D. 1993. High ground displacement velocities associated with rockburst damage. (*In: Young. Rockbursts and Seismicity in Mines.* Rotterdam: Balkema)

Wagner, H. 1984. Support required for rockburst conditions. (*In: Gay, NC and Wainwright, EH, Proceedings of the 1st International Congress on Rockbursts and Seismicity in Mines,* Johannesburg, 1982. SAIMM. Johannesburg).

Appendix 1: Data

Table A1. Parameters of Driefontein Mine records

		F	H	H	Dis	X	Y	Z	Ma	Mom	Ene
		[m/ss]	[m/ss]	[m/ss]	[m]	[m]	[m]	[m]		log	log
										[Nm]	[J]
08Sep	14:24:26	27	10	13							
08Sep	14:24:27	53	17	26		18660	-10240	-2275		11.7	6.7
09Sep	01:37:52	14	8	9		18910	-10395	-2251		10.2	4.8
09Sep	18:05:17	12	6	8							
11Sep	15:42:28	11	5	5							
11Sep	16:11:12	58	3	3		Two	Events				
12Sep	15:15:51	120	8	15							
12Sep	15:15:54	6	6	5							
12Sep	15:16:00	200	7	10							
12Sep	15:16:18	74	3	3							
12Sep	15:16:27	67	2	7							
13Sep	14:05:21	7	5	4		18894	-10398	-2263		11.1	5.7
26Sep	01:14:20	15	20	3							
27Sep	08:24:14	12	8	3							
27Sep	16:43:23	87	12	5		18735	-10326	-2396		8.6	3.1
27Sep	16:44:45	6	8	3		18726	-10348	-2419		8.6	2.8
27Sep	23:18:41	8	7	7							
		H-V	H-H1	H-H2							
29Sep	15:34:35	76	118	102	87	18679	-10287	-2267	2.0	12.3	7.3
		H	F	F							
17Oct	13:28:31	10	13	8							
18Oct	14:21:00	14	16	4		18927	-10259	-2589		10.5	4.9
!8Oct	14:55:07	9	12	16							

Table A2. Parameters of Driefontein Main records

		H	S	F	Dis	X	Y	Z	Ma	Mom	Ene
2001		[m/ss]	[m/ss]	[m/ss]	[m]	[m]	[m]	[m]		Log	log
										[Nm]	[J]
06Jan	12:41:47	12	18	6							
09Jan	13:35:41	7	13	3							
09Jan	13:35:53	11	16	3							
09Jan	13:36:28	5	8	2							
09Jan	13:49:09	3	1	3							
10Jan	08:45:13	12	14	14							
12Jan	09:44:01	12	1	1							
12Jan	09:44	29	35	94							
12Jan	13:48:44	6	6	13		18956	-10346	-2381	1.8	11.8	6.5
12Jan	14:38:44	13	10	19							
12Jan	14:39:48	120	210	110		Impuls					
12Jan	14:44:25	5	6	11							
12Jan	14:44:35	3	6	10							
12Jan	17:33:44	4	4	13		18495	-10267	-2240	1.7	11.6	6.5
13Jan	14:24:15	89	71	43		18664	-10314	-2242	2.6	12.8	8.0
14Jan	23:52:40	2	5	20							
15Jan	14:02:25	4	7	10							
15Jan	14:02:17	4	5	17							

15Jan	14:02:34	3	6	11							
16Jan	15:46:21	16	13	6							
23Jan	15:58:45	5	12	2							
24Jan	15:14	8	6	2							
24Jan	16:15	8	7	3							
24Jan	16:16	6	7	3							
25Jan	12:38:09	5	9	13							
25Jan	12:38:09	2	10	11							
25Jan	12:38:58	2	7	9							
26Jan	13:59:30	10	5	12							
26Jan	14:00	5	9	5							
26Jan	14:00:17	11	12	3							
26Jan	14:00:54	7	7	4							
26Jan	14:30:36	17	20	6							
27Jan	11:56:46	8	6	15							
27Jan	14:41	5	9	10							
27Jan	17:35:52	21	22	49							
27Jan	17:43:16	8	9	11							
27Jan	17:48:15	14	9	22							
31Jan	14:47	8	12	2							

Table A3. Parameters of Mponeng Mine records

		F	F	H	Dis	X	Y	Z	Mag	Mom	Ene
2000		**[m/ss]**	**[m/ss]**	**[m/ss]**	**[m]**	**[m]**	**[m]**	**[m]**		**Log**	**log**
										[Nm]	**[J]**
24Oct	17:38:48	8	8	12	76	30075	-41934	2885	0.7	10.5	4.6
24Oct	17:38:51	6	8	12	82	30081	-41911	2895	1.1	11.2	5
25Oct	18:40:31	26	20	29	159	30003	-42094	2896	1.7	11.7	6.1
26Oct	00:32:57	7	7	14	103	30094	-41972	2845	1	10.9	5.1
26Oct	05:14:12	30	22	12	75	30141	-42010	2991	1.3	11.3	5.4
		S	**F**	**H**							
30Oct	17:29:00	25	6	13	68	30067	-41986	2886	0.7		
31Oct	17:05:00	16	14	14	156	30104	-42093	2849	1.2		
6Nov	16:56:03	48	24	16	197	30183	-42108	2837	0.4	10.4	3.8
6Nov	16:56:09	22	8	15	172	30183	-42053	2825	0.4	10.1	4.1
6Nov	22:09:07	29	32	18							
6Nov	22:17:23	29	44	36	65	30128	-41943	2994	1.4	11.5	5.8
7Nov	15:41:30	25	21	20							
7Nov	16:35:41	27	11	12	151	30212	-42061	2977	0.7	10.8	4.2
7Nov	17:01:27	76	77	25	77	30153	-41966	2995	1.2	11.2	5.4
7Nov	17:55:29	6	5	5	127	30140	-41947	2833	0.2	9.9	3.8
8Nov	15:23:00	12	15	13	62	30138	-41995	2984	0.5	10.4	4
8Nov	15:23:03	17	20	13	79	30119	-42037	2910	0.5	10.2	4.4
8Nov	15:23:05	50	34	23	124	30191	-42035	2905	0.9	10.9	4.7
8Nov	15:47:08	7	9	3							
9Nov	15:51:08	33	31	11	70	30076	-42028	2989	0.8	10.6	4.9
		29									
		25									
11Nov	15:18:31	46	77	20	141	30176	-42077	2995	0.7	10.6	4.4
		33									
		51									
11Nov	15:18:31	20	20	17	67	30056	-42028	2963	0.5	10.3	4.2
		24									

		19									
14Nov	08:43:21	15			125	30184	-42019	3020	1.9	`12.1	6.3
		12									
15Nov	16:35:32	6	12	10	70	30155	-41943	2940	0.7	10.7	4.3
		14									
		16									
15Nov	17:18:43	13	7	10	223	30313	-41943	2940	0.8	10.7	4.8
		24									
		11									
16Nov	15:06:00	3	2	2	157	30219	-42038	2881	0	9.7	3.5
	15:06:03	6			186	30197	-42126	2929	0.9	11	4.5
		2									
17Nov	15:17:48	8	9	3		Series					
	15:17:52	12	20	15		Series					
	15:19:37				160	30185	-42094	2998	0.6		
17Nov	18:12:52	18	38	30	90	30100	-41958	2859	1.7	11.9	6.1
		19									
		32									
20Nov	07:54:55	5	9	4							
21Nov	12:16:52	6	14	6							
21Nov	15:58:24	3	5	2	235	30254	-42108	2844	0.5	10.4	4.2
21Nov	15:58:28	4	7	3	206	30243	-42087	2866	0.5	10.5	4
21Nov	15:59:57	19	24	12	112	30187	-42024	2980	1.1	11.2	5.1
21Nov		7	7	4							
		4	4	2							
21Nov	22:18:44	11	24	8	62	30108	-41997	2893	0.1	10	3.5
		10									
		13									
22Nov	03:00:50	8	14	6							
		8									
		14									
22Nov	08:11:37	4	5	2	180	30179	-42104	2859	0.1	9.8	3.6
25Nov	11:25:22	100	55	22	69	30151	-41968	2985	1.2	11.3	5.2
		55									
		91									
27Nov	20:24:00	11	10	19							
		8									
		9									
28Nov	05:03:04	20	11	22	215	30307	-41971	2949	1.7	11.6	6.5
		25									
		11									
1Dec	17:07:00	28	17	14	134	30179	-42017	3040	1.3	11.5	5.4
1Dec	21:32:06	3	4	3	116	30150	-42074	2940	0	9.5	3.7
2Dec	14:37:01	3	4	9	195	30262	-41913	2873	0.1	9.6	3.7
4Dec	17:19:56	3	3	3	108	30180	-42030	2974	0.6	10.7	3.9
4Dec	17:22:58	63	39	76	142	30146	-42024	2826	2.4	12.5	7.4
4Dec	17:22:58	5	4	3	100	30170	-41964	3011	0.1	9.9	3.6
4Dec	17:36:44	3	1	2	100	30149	-42052	2923	0.4	10.6	3.6
4Dec	20:56:18	5	3	6	65	30054	-41938	2908	0.6	10.3	4.6
4Dec	21:42:22	5	1	3							
4Dec	23:59:18	4	2	5							
5Dec	02:12:35	16	13	11							
5Dec	07:40:54	12	7	7							
6Dec	06:14:57	4	5	3	146	30217	-42045	2922	1	10.8	5.5

7Dec	11:41:36	7	7	11							
8Dec	15:37:41	3	3	2	225	30270	-42094	2882	0.6	10.6	4.1
8Dec	15:50:16	5	4	3	160	30224	-42042	3007	1.2	11.4	5.3
11Dec	15:40:54	11	10	4	165	30217	-42069	2997	1.7	12	5.9
14Dec	15:33:00				165	30235	-42057	2948	0.7	10.5	4.7
14Dec	15:35:23				89	30126	-42054	2965	0.4	9.2	2.5
14Dec	16:38:00	24	7;19	13							
		43									
15Dec	17:18:31	-	25;23	9	135	30185	-42067	2979	0.9	10.8	4.8
		-									
15Dec	21:06:32	15	11	5							
16Dec	1:42:22	11	7	4							
16Dec	20:24:31	17	11;16	19	76	30134	-42037	2941	-0.1	9.5	3.3
		39									
17Dec	20:37:35	11	4;8	4							
		15									
18Dec	16:22:23	81	22-91	43	165	30242	-42043	2941	1.8	12.1	6.3
		85									
19Dec	23:58:57				223	30312	-41942	2926	1.8	11.8	6.5
20Dec	16:59:39	-	18;27	55	223	30256	-42026	2915	0.8	10.9	10.9
		-									
20Dec	20:09:04	18	4;4	12	104	30167	-42046	2948	-0.4	9.3	2.4
		18									
20Dec	20:49:14	16	2;3	9							
		17									
28Dec	16:09:23	20	11	12		30220	-42063	3025	0.1	9.9	3.5
29Dec	15:20	17	19	23							
29Dec	15:40:06	15	5	6		30193	-42047	2955	0.4	10.2	4.1
29Dec	15:57	9	5	6							
29Dec	17:41:10	20	27	12		30241	-42032	2939	0.7	10.7	4.3
29Dec	17:45	10	15	13							
30Dec	15:45:35	17	11	15		30270	-41955	2936	-0.6	9.0	2.4
30Dec	19:15:29	29	19	15		30197	-42095	2961	0.3	10.1	3.8
30Dec	19:18	31	18	18							
02Jan	16:23	15	7	17							
02Jan	16:23	33	21	11							
03Jan	01:56:08	17	12	11		30221	-42087	2900	-0.4	9.3	2.7
03Jan	16:33:30	94	29	35							
03Jan	20:10:33	15	8	12		30197	-42067	2991	0.9	10.6	5.1
04Jan	01:07:43	13	11	8							
04Jan	17:35:25	38	26	20		30277	-42046	2895	0.7	10.9	4.2
08Jan	21:14:29	20	30	20		30207	-42056	2979	0.3	10.1	3.7
08Jan	18:09:49	26	15	35		30207	-42056	2979	0.3	10.2	3.8
10Jan	17:03:49	8	10	9		30225	-42075	2924	0.4	10.3	3.8
10Jan	19:06:54	8	13	20		30232	-42091	2973	1.1	11.1	5.2
12Jan	9:32:20	19	12	11		30210	-42049	3007	1.3	11.4	5.4
15Jan	17:20:19	40	15	24		30260	-42049	2981	1.5	11.7	5.6
28Jan	04:00:17	4	7	5							
29Jan	18:34:16	5	10	8							
30Jan	18:09:42	8	12	12							

Appendix 2: Numerical Integration of ground motion

Velocity of ground motion is obtained by the integration of an accelerogram and in the same way displacement of ground motion is resolved from velocity of ground motion. Integration is completed using the widely recommended method of Newmark.

Integration of seismic records is a very unstable task due to a presence of noise in the signal. The process of integration cumulates with time low-frequency noise present in the accelerograms. It is not difficult to remove this characteristic effect using high pass filters, but usually corrections deform the shape of the original signal.

Therefore, it is better to use a short time series to reduce the negative effect of integration or long time series before the arrival of a seismic event and subtract polynomial, that is responsible for the destroying of zero level line. Several tests with different parameters of integration routine would allow the development of confidence in calculation of velocity of ground motion, values of peak ground velocity, PGV, peak ground displacement, PGD and other major features of waveforms.

The most delicate matter is the interpretation of final displacement after dynamic ground motion finished. The resulting displacement is sensitive to the choice of the technique. Tests with synthetic noisy data show that it is possible to mistake the long period response for underlying long period noise. Likely, the final displacement exhibits several features, which allow separate artificial effect from the real one. The final displacement should be smaller than dynamic displacement, and should be constant over time. Finally, it is expected that most weak ground motions will have zero final displacement and the strong ground motion will yield final displacement, which is proportional to dynamic parameters of ground motion. Dominant pulses of velocity of ground motion for strong ground motion are distinctive. Visual inspection of velocity of ground motion reveals asymmetry of the waveform with respect to the zero line. This asymmetry indicates that final displacement is not zero.